



TOI-4504: Exceptionally Large Transit Timing Variations Induced by Two Resonant Warm Gas Giants in a Three-planet System

Michaela Vítková^{1,2} , Rafael Brahm^{3,4,5} , Trifon Trifonov^{6,7,8} , Petr Kabáth¹ , Andrés Jordán^{3,4,5} , Thomas Henning⁶ , Melissa J. Hobson⁹ , Jan Eberhardt⁶ , Marcelo Tala Pinto³ , Felipe I. Rojas¹⁰ , Nestor Espinoza¹¹ , Martin Schlecker¹² , Matías I. Jones¹³ , Maximiliano Moyano¹⁴ , Susana Eyheramendy^{3,4,5} , Carl Ziegler¹⁵ , Jack J. Lissauer¹⁶ , Andrew Vanderburg¹⁷ , Karen A. Collins¹⁸ , Bill Wohler¹⁹ , David Watanabe²⁰ , George R. Ricker²¹ , Roland Vanderspek²¹ , Sara Seager^{21,22,23} , Joshua N. Winn²⁴ , Jon M. Jenkins¹⁶ , and Marek Skarka^{1,2}

¹ Astronomical Institute of the Czech Academy of Sciences, Fričova 298, CZ-25165 Ondřejov, Czech Republic; vilkova@asu.cas.cz
² Department of Theoretical Physics and Astrophysics, Faculty of Science, Masaryk University, Kotlářská 2, CZ-61137 Brno, Czech Republic

³ Facultad de Ingeniería y Ciencias, Universidad Adolfo Ibáñez, Av. Diagonal las Torres 2640, Peñalolén, Santiago, Chile

⁴ Millennium Institute for Astrophysics, Chile

⁵ Data Observatory Foundation, Chile

⁶ Max-Planck-Institut für Astronomie, Königstuhl 17, D-69117 Heidelberg, Germany

⁷ Department of Astronomy, Sofia University "St Kliment Ohridski," 5 James Bourchier Boulevard, BG-1164 Sofia, Bulgaria

⁸ Landessternwarte, Zentrum für Astronomie der Universität Heidelberg, Königstuhl 12, D-69117 Heidelberg, Germany

⁹ Observatoire de Genève, Département d'Astronomie, Université de Genève, Chemin Pegasi 51b, 1290 Versoix, Switzerland

¹⁰ Instituto de Astrofísica, Facultad de Física, Pontificia Universidad Católica de Chile, Chile

¹¹ Space Telescope Science Institute, 3700 San Martin Drive, Baltimore, MD 21218, USA

¹² Department of Astronomy/Steward Observatory, The University of Arizona, 933 North Cherry Avenue, Tucson, AZ 85721, USA

¹³ European Southern Observatory, Alonso de Córdova 3107, Vitacura, Casilla 19001, Santiago, Chile

¹⁴ Instituto de Astronomía, Universidad Católica del Norte, Angamos 0610, 1270709, Antofagasta, Chile

¹⁵ Department of Physics, Engineering and Astronomy, Stephen F. Austin State University, 1936 North Street, Nacogdoches, TX 75962, USA

¹⁶ NASA Ames Research Center, Moffett Field, CA 94035, USA

¹⁷ Department of Astronomy, University of Wisconsin–Madison, Madison, WI 53706, USA

¹⁸ Center for Astrophysics | Harvard & Smithsonian, 60 Garden Street, Cambridge, MA 02138, USA

¹⁹ SETI Institute, Mountain View, CA 94043 USA/NASA Ames Research Center, Moffett Field, CA 94035, USA

²⁰ Planetary Discoveries, Valencia, CA 91354, USA

²¹ Department of Physics and Kavli Institute for Astrophysics and Space Research, Massachusetts Institute of Technology, 77 Massachusetts Avenue, Cambridge, MA 02139, USA

²² Department of Earth, Atmospheric and Planetary Sciences, Massachusetts Institute of Technology, 77 Massachusetts Avenue, Cambridge, MA 02139, USA

²³ Department of Aeronautics and Astronautics, Massachusetts Institute of Technology, 77 Massachusetts Avenue, Cambridge, MA 02139, USA

²⁴ Department of Astrophysical Sciences, Princeton University, Princeton, NJ 08544, USA

Received 2024 September 11; revised 2024 December 02; accepted 2024 December 03; published 2025 January 3

Abstract

We present a joint analysis of transit timing variations (TTVs) and Doppler data for the transiting exoplanet system TOI-4504. TOI-4504 c is a warm Jupiter-mass planet that exhibits the largest known TTVs, with a peak-to-node amplitude of ~ 2 days, the largest value ever observed, and a superperiod of ~ 930 days. TOI-4504 b and c were identified in public Transiting Exoplanet Survey Satellite (TESS) data, while the TTVs observed in TOI-4504 c, together with radial velocity (RV) data collected with FEROS, allowed us to uncover a third, nontransiting planet in this system, TOI-4504 d. We were able to detect transits of TOI-4504 b in the TESS data with a period of 2.4261 ± 0.0001 days and derive a radius of $2.69 \pm 0.19 R_{\oplus}$. The RV scatter of TOI-4504 was too large to constrain the mass of TOI-4504 b, but the RV signals of TOI-4504 c and d were sufficiently large to measure their masses. The TTV+RV dynamical model we apply confirms TOI-4504 c as a warm Jupiter planet with an oscillating period of 82.54 ± 0.02 days, a mass of $3.77 \pm 0.18 M_J$, and a radius of $0.99 \pm 0.05 R_J$, while the nontransiting planet TOI-4504 d has an orbital period of 40.56 ± 0.04 days and a mass of $1.42^{+0.07}_{-0.06} M_J$. We present the discovery of a system with three exoplanets: a hot sub-Neptune and two warm Jupiter planets. The gas giant pair is stable and likely locked in a first-order 2:1 mean-motion resonance (MMR). The TOI-4504 system is an important addition to MMR pairs, whose increasing occurrence supports a smooth migration into a resonant configuration during the protoplanetary disk phase.

Unified Astronomy Thesaurus concepts: Exoplanet dynamics (490); Transit photometry (1709); Transit timing variation method (1710); Radial velocity (1332)

1. Introduction

More than 5000 transiting exoplanets have been identified. In a Keplerian system, transits occur at regular intervals. However,

if additional planets are present in a system and their gravitational interactions are significant on observable time-scales, then transit timing variations (TTVs; A. R. Dobrovolskis & W. J. Borucki 1996; J. Miralda-Escudé 2002) are expected over the observed baseline. In particular, planets in or near low-order mean-motion resonances (MMRs) exhibit the largest TTV signals (E. Agol et al. 2005). TTVs provide important constraints on the planetary masses and orbital parameters in the system and



Original content from this work may be used under the terms of the [Creative Commons Attribution 4.0 licence](https://creativecommons.org/licenses/by/4.0/). Any further distribution of this work must maintain attribution to the author(s) and the title of the work, journal citation and DOI.

sometimes help uncover nontransiting planets. For instance, the first nontransiting planet fully characterized through TTVs was Kepler-46 c (D. Nesvorný et al. 2012), which induced TTVs on the transiting planet Kepler-46 b. Another example is Kepler-88 b, with a TTV amplitude of approximately 12 hr (peak to node), earning it the title “the King of TTVs” (D. Nesvorný et al. 2013). These TTVs revealed a pair of planets near the 2:1 MMRs. Another case of 2:1 resonance causing the peak-to-node TTVs of ~ 1 day can be seen in Kepler-30 b (B. Tingley et al. 2011; F. Panichi et al. 2018). Kepler-90 g has a variation of 25.7 hr in the time lapsed between consecutive transits, but only a few transits have been observed, and the full amplitude of variation is not known (J. Cabrera et al. 2014).

Currently, we know of 30 planets discovered by TTVs,²⁵ and more are being detected by NASA’s Transiting Exoplanet Survey Satellite (TESS; G. R. Ricker et al. 2015). TESS aims to detect transiting planets around relatively bright stars that are suitable for precise radial velocity (RV) measurements and, in rare cases, could help uncover nontransiting planets through TTVs. A combination of precise RV measurements and TTVs helps determine the planetary mass, radius, bulk density, and other important physical parameters.

In this work, we confirm the exoplanetary nature of the detected signal from TOI-4504. We firmly validate TOI-4504 c and report evidence for a nontransiting planet, TOI-4504 d, that causes very strong TTVs of TOI-4504 c. TOI-4504.01 (hereafter TOI-4504 c) was identified by the Warm GIAnTs with tEss collaboration, which is dedicated to the systematic characterization of TESS transiting warm giant planets (see, e.g., R. Brahm et al. 2019; A. Jordn et al. 2020; M. Schlecker et al. 2020; M. J. Hobson et al. 2021, 2023; T. Trifonov et al. 2021; V. Bozhilov et al. 2023; M. I. Jones et al. 2024, and references therein). The signature was referred to the TESS Science Office at MIT as a CTOI in 2020 May, and the Quick Look Pipeline (C. X. Huang et al. 2020a, 2020b) was run to assess the candidate, identifying a period of $P = 81.966$ days. The TESS Science Processing Operations Center (SPOC; J. M. Jenkins et al. 2016) independently detected transits of TOI-4504 c in sector 34 and several subsequent single- and multisector searches using a noise-compensating matched filter (J. M. Jenkins 2002; J. M. Jenkins et al. 2020), and an initial limb-darkened transit model was fit (J. Li et al. 2019) and a suite of diagnostic tests were conducted to help make or break the planetary interpretation (J. D. Twicken et al. 2018). The shallower signal designated as TOI-4504.02 (hereafter TOI-4504 b) was detected by the TESS SPOC (J. M. Jenkins et al. 2016) at the NASA Ames Research Center with $P = 2.4261$ days in a search of sectors 27–36. Both TOI-4504 b and c were alerted to the community by the TESS Science Office on 2021 October 21.

In this work, we report evidence for a nontransiting planet, TOI-4504 d, that causes very strong TTVs of TOI-4504 c. The induced TTVs on TOI-4504 c have a semiamplitude of a little less than 2 days (peak-to-peak of 4 days), making TOI-4504 c a new record holder for TTV signal amplitude. Given the strong sinusoidal TTV signal we detect, near a low-order period ratio, commensurability with the transiting planet is suspected. In such cases, the TTV periodic signal can be approximated by the

so-called “superperiod,”

$$P_{\text{TTV}} = \left| \frac{j-1}{P_{\text{in}}} - \frac{j}{P_{\text{out}}} \right|^{-1}, \quad (1)$$

where $j = P_{\text{out}}/P_{\text{in}}$ represents the close commensurability between the inner and the outer planets. The observed superperiod of TOI-4504 is ~ 930 days. Our fitting analysis of the observed data indicates that TOI-4504 d is an inner Jovian-mass planet with a period of about 41 days, placing it in a 2:1 period ratio commensurability with the transiting exoplanet TOI-4504 c.

This paper is organized as follows. In Section 2, we introduce the photometric and spectroscopic data collected for TOI-4504. In Section 3, we present the stellar parameters of TOI-4504. In Section 4, we introduce our orbital analysis and results. Finally, in Section 5, we present a summary and our conclusions.

2. Observations

2.1. TESS Photometry

TOI-4504 was observed with a 30 minute cadence during the first year of the TESS primary mission in sectors 1–13. In the third and fifth years (sectors 27–38, 61–65, and 67–69), it was observed with a 120 s cadence. The image data were reduced and analyzed by the SPOC at the NASA Ames Research Center.

We retrieved the 30 minute data using the Tesseract pipeline²⁶ (F. Rojas et al. 2024, in preparation). This pipeline extracts light curves from full-frame images using the TESSCut (C. E. Brasseur et al. 2019) and Lightkurve (Lightkurve Collaboration et al. 2018) packages. The download of the data with a 120 s cadence was done with Lightkurve. Transits of TOI-4504 c occur in sectors 3, 6, 9, 12, 28, 31, 34, 37, 61, 64, and 67. We used the Presearch Data Conditioning Simple Aperture Photometry (PDCSAP) flux (J. C. Smith et al. 2012; M. C. Stumpe et al. 2012, 2014) in all sectors where it is available. PDCSAP light curves are corrected for systematic trends. The transit present in sector 61 is cut off by a quality check in PDCSAP. This transit can be seen in simple aperture photometry data but is contaminated by background noise. It was possible to use data from this sector for measuring the TOI-4504 c transit time, but we did not use these data to fit the planet parameters. Analysis of TOI-4504 c is described in more detail in Section 4.1.2.

For the TOI-4504 b analysis, we used 120 s cadence data available in sectors 27–38, 61–65, and 67–69 and PDCSAP light curves. Analysis of TOI-4504 c is described in Section 4.1.1.

2.2. Spectroscopic Data

Follow-up observations of TOI-4504 were performed with the FEROS spectrograph (A. Kaufer et al. 1999) mounted at the Max Planck Gesellschaft 2.2 m telescope at La Silla Observatory. TOI-4504 was observed between 2020 March and 2024 May in order to validate the transiting companions and constrain their masses. We obtained 39 spectra with exposure times of 1500 and 1800 s and an average signal-to-noise ratio of 40. We used the Ceres pipeline (R. Brahm et al. 2017a) to process the data. From this pipeline, we obtained RV and

²⁵ NASA Exoplanet Archive, 2024 September 3: <https://exoplanetarchive.ipac.caltech.edu>.

²⁶ Available at <https://github.com/astrofelipe/tesseract>.

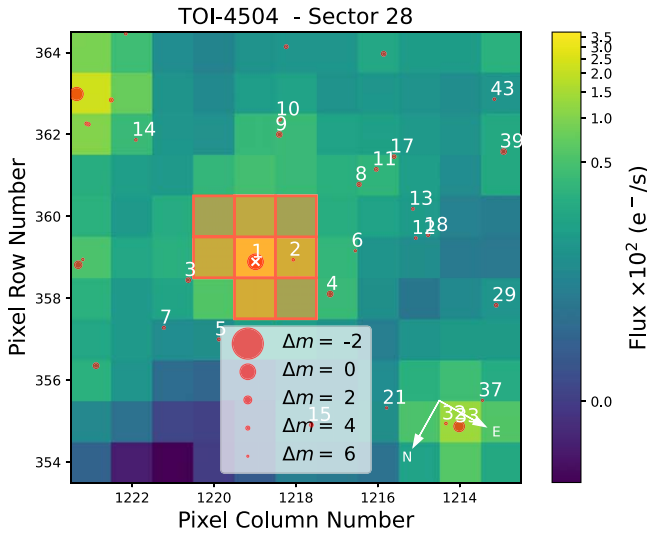


Figure 1. TPFs in sector 28 for TOI-4504 obtained with Tpfplotter. The shape of the aperture mask used to extract the photometry is marked with orange. Red dots indicate the sources of the Gaia DR3 catalog in the field. TOI-4504 is marked with a white cross.

stellar activity indicators such as cross-correlation function bisector spans (BIS; e.g., D. Queloz et al. 2001), H_α (I. Boisse et al. 2009), $\log(R'_{HK})$ (R. W. Noyes et al. 1984; D. K. Duncan et al. 1991), Na II, and He I (J. Gomes da Silva et al. 2011). Our extracted RVs and activity indices for TOI-4504 are listed in Table A3.

2.3. Inspection of Nearby Sources

For inspection of target pixel files (TPFs), we used Tpfplotter (A. Aller et al. 2020). It compares the Gaia DR3 catalog with the TESS TPF and allows us to see possible contamination in the field. In Figure 1, a TPF image of sector 28 is shown. In almost all sectors, a star with Gaia ID 5289275864525442048 (TIC 349972416, $G = 18.48$ mag; star 2 in Figure 1) is in the aperture mask. It is 5.4 mag fainter than our object, and the distance between our target and TIC 349972416 is $19''.37$. Among the multiple-sector data, there are two additional sources, 3 and 4, which are often close to or in the aperture; however, if the transit events were on the possible contaminator stars, the transit depth would vary substantially in the observed sectors, which were not observed. Our RVs show that the transits likely originate from the target star and not from this companion (Section 2.2).

To reject the contamination by sources closer than $\sim 2''$ from the target star, we used the 4.1 m SOAR telescope (A. Tokovinin 2018) within the SOAR TESS survey (C. Ziegler et al. 2019) to obtain speckle imaging. The images were obtained on 2022 April 15 with a Cousins I filter and a resolution of 36 mas, and they did not reveal any nearby sources. In Figure 2, the speckle autocorrelation function and the contrast curve are shown. It reaches a contrast of $\Delta\text{mag} = 4.5$ at $0''.5$, and an estimated point-spread function is $0''.064$. There is no apparent nearby contaminant within $3''$ from the target (Figure 2). Furthermore, the Gaia renormalized unit weight error value of 1.12 of our object also indicates that the single-star model fits the astrometric observations well. Additionally, the SPOC difference image centroid test was able to localize the host star to within $0''.33 \pm 2''.7$ of the transit source location (averaged over the different TESS threshold crossing event in the S27-69 search) for TOI-4504 c and $1''.8 \pm 3''.1$

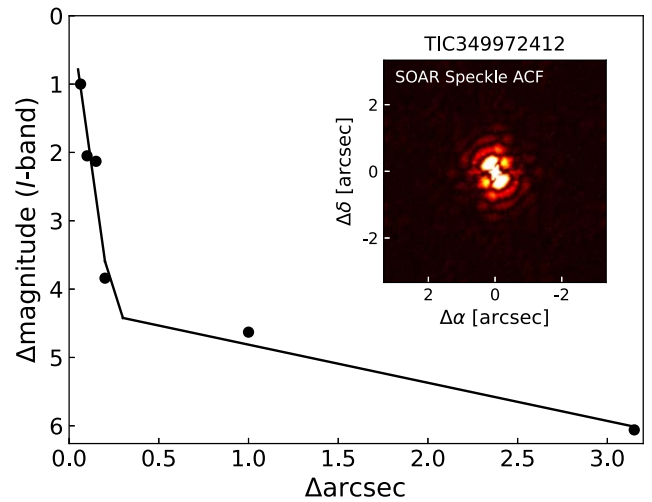


Figure 2. High-resolution imaging from SOAR for TOI-4504. The inside image shows a speckle autocorrelation function. The 5σ contrast curve is shown as the black points with the linear fit as the black solid line.

of the transit source location for TOI-4504 b (based on the S27-69 search).

2.4. Follow-up Photometry

Several follow-up photometric observations of TOI-4504 c were conducted and are available in ExoFOP. Eight observations were scheduled to record the transit of TOI-4504 c, assuming a constant period, but all resulted in nondetections. The nondetections, potentially due to the large TTVs, make it harder to predict the next transit. We include our predictions for upcoming transits in the Appendix. There are two observations of TOI-4504 b, but since this exoplanet does not directly contribute to the detected TTVs aimed to be studied in this work, this observation was excluded from the modeling scheme.

We conclude that TOI-4504 is a metal-rich ($[\text{Fe}/\text{H}] = 0.16 \pm 0.05$ dex) main-sequence star ($M_* = 0.89^{+0.06}_{-0.04} M_\odot$, $R_* = 0.92^{+0.04}_{-0.04} R_\odot$), just on the boundary between a G- and a K-type star ($T_{\text{eff}} = 5315 \pm 60$ K).

3. Stellar Parameters of TOI-4504

We followed the two-step iterative procedure presented in R. Brahm et al. (2019) to obtain the stellar parameters of the host star. We start from the coadded FEROS spectra to obtain the stellar atmospheric parameters (T_{eff} , $\log g$, $[\text{Fe}/\text{H}]$, $v \sin i$) using the ZASPE package (R. Brahm et al. 2017b). We perform a spectral energy distribution fit to estimate the stellar physical parameters, using the publicly available broadband photometry as data and the PARSEC isochrones as a model. This step involved the use of the Gaia DR3 (Gaia Collaboration et al. 2023) parallax to convert the observed apparent magnitudes to absolute magnitudes and adopt a simple interstellar extinction rule (J. A. Cardelli et al. 1989).

We also fix the metallicity to the one derived with ZASPE and use the ZASPE value for the T_{eff} as a prior. This step produces a more precise value for the stellar $\log g$, which is used as input in a new run of ZASPE. We continue with the iterations until reaching convergence of the T_{eff} and $[\text{Fe}/\text{H}]$ in two subsequent ZASPE runs. Stellar parameters from our analysis are listed in Table 1. The uncertainties in the stellar

Table 1
Stellar Parameters of TOI-4504

Parameter	Value	Reference
Names	TIC 349972412, TOI-4504	TIC v8.2
R.A. (J2000)	07 ^h 37 ^m 52 ^s .1529498945	Gaia DR3
Decl. (J2000)	−62°04′41″.803583657	Gaia DR3
T (mag)	12.5542	TIC v8.2
B (mag)	14.239	TIC v8.2
V (mag)	13.364	TIC v8.2
Distance (pc)	342.605 ± 1.707	TIC v8.2
Spectral type	K1V	P&M
T_{eff} (K)	5315 ± 60	This work
$\log g$ (cm s ^{−2})	4.458 ^{+0.021} _{−0.015}	This work
R_* (R_\odot)	0.92 ^{+0.04} _{−0.04}	This work
M_* (M_\odot)	0.89 ^{+0.06} _{−0.04}	This work
L_* (L_\odot)	0.62 ^{+0.03} _{−0.03}	This work
ρ_* (kg m ^{−3})	1607 ⁺⁹³ _{−64}	This work
[Fe/H] (dex)	0.16 ± 0.05	This work
$v \sin i$ (km s ^{−1})	1.9 ± 0.5	This work
Age (Gyr)	10.0 ^{+2.9} _{−3.6}	This work
A_V (mag)	0.35 ^{+0.07} _{−0.06}	This work

Note. P&M: M. J. Pecaut & E. E. Mamajek (2013); TIC v8.2: K. G. Stassun et al. (2019), M. Paegert et al. (2022); Gaia DR3: Gaia Collaboration et al. (2016, 2023).

parameters obtained with our procedure do not include possible systematic differences with respect to other stellar models; because of this, we inflate the uncertainties as suggested in J. Tayar et al. (2022).

4. Analysis and Results

4.1. Transit Analysis and TTV Extraction

For the transit fitting, we used the python package Juliet (N. Espinoza et al. 2019), which employs transit light-curve models from the Batman package (L. Kreidberg 2015). Transit analysis of each planet was treated individually.

4.1.1. TOI-4504 b

For the transit analysis of TOI-4504 b, we used 2 minute PDCSAP data. Before the analysis, we deleted transits of TOI-4504 c from the time series. We used broad uninformative priors (see Table 2). The final values of the fit are also listed in Table 2.

Figure 3 shows binned data that are phase-folded with the orbital period of 2.42614 days together with the fit of the transit. We detected a planet with a transit depth of $\Delta F = 718$ ppm. Our RV data were insufficient to confirm this planet and estimate its mass (see Section 4.2). However, the radius of $R_p = 2.691 \pm 0.191 R_\oplus$ and mass of $10.4 \pm 0.9 M_\oplus$ calculated from the mass–radius relations (S. Müller et al. 2024) point toward the classification of planet b as a sub-Neptune. We did not detect TTVs in TOI-4504 b.

4.1.2. TOI-4504 c

To extract TOI-4504 c TTVs, we again used Juliet. First, we detrended the light curves of all sectors containing transits of TOI-4504 c. We used the Gaussian process (GP) on the out-of-transit data to remove trends in each TESS sector before fitting

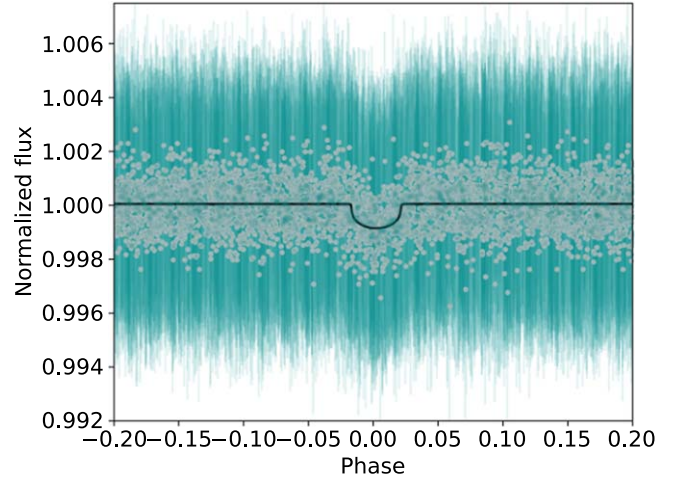


Figure 3. Phase plot for TOI-4504 b transit. The light curve was binned into 1 hr bins.

Table 2
Priors and Posteriors for TOI-4504 b Parameters Derived with Juliet

Parameter	Prior	Posterior
P (days)	$\mathcal{N}(2.4, 0.5)$	2.42614 ^{+0.00014} _{−0.00013}
t_0 (BJD)	$\mathcal{N}(2459038.46, 0.2)$	2459038.458 ^{+0.022} _{−0.021}
b	$\mathcal{U}(0.0, 1.0)$	0.396 ^{+0.134} _{−0.197}
R_p/R_*	$\mathcal{U}(0.0, 1.0)$	0.0268 ^{+0.0019} _{−0.0019}
q_1	$\mathcal{U}(0.0, 1.0)$	0.527 ^{+0.320} _{−0.308}
q_2	$\mathcal{U}(0.0, 1.0)$	0.496 ^{+0.323} _{−0.316}
e	Fixed 0.0	...
ω (deg)	Fixed 90.0	...
ρ_* (kg cm ^{−3})	$\mathcal{N}(1600, 100)$	1601 ⁺¹⁰⁰ _{−97}
m_{dilution}	Fixed 1.0	...
m_{flux}	$\mathcal{N}(0.0, 0.1)$	−0.000046 ^{+0.000014} _{−0.000014}
σ_w (ppm)	$\mathcal{J}(0.1, 1000.0)$	2.16 ^{+17.11} _{−1.90}
a (au)	...	0.03392 ± 0.00068
R_p (R_\oplus)	...	2.691 ± 0.191
i (deg)	...	87.4 ^{+0.9} _{−1.3}

Note. a is calculated using Kepler's third law and derived period P .

the planet parameters. The GP model utilizes an approximate Matern kernel from Celerite (D. Foreman-Mackey et al. 2017).

We used wide priors for an amplitude of the GP $\sigma_{\text{GP,TESS}}$ of $\mathcal{J}(10^{-6}, 10^6)$, where $\mathcal{J}(a, b)$ represents a Jeffreys prior between a and b . For the time/length scale of the GP $\rho_{\text{GP,TESS}}$, we used $\mathcal{J}(10^{-3}, 10^3)$. The fit was done using priors for the instrumental parameters, namely, the flux offset m_{flux} , jitter σ_w , dilution factor m_{dilution} , and limb-darkening coefficients q_1 and q_2 . For the planetary parameters, we used parameterization using the planet-to-star radius ratio p and impact parameter b . Priors for eccentricity e and argument of periastron ω were fixed to 0 and 90°, respectively.

The RV data showed no indication of a significant eccentricity. Thus, fixed eccentricity is sufficient for TTV determination. Priors for transit times $T_{\text{transit number}}$ were determined visually from the light curve because of the strong TTVs. All priors and posteriors for the complete fit are listed in Table 3. A zoom-in for the fit of the transits is shown in Figure 4.

Table 3
Priors and Posteriors for the TTV Extraction with Juliet for TOI-4504 c

Parameter	Prior	Posterior
b	\mathcal{U} (0.0, 1.0)	$0.492^{+0.038}_{-0.041}$
R_p/R_*	\mathcal{U} (0.0, 1.0)	$0.108^{+0.001}_{-0.001}$
q_1	\mathcal{U} (0.0, 1.0)	$0.426^{+0.114}_{-0.125}$
q_2	\mathcal{U} (0.0, 1.0)	$0.203^{+0.094}_{-0.091}$
e	Fixed 0.0	...
ω (deg)	Fixed 90.0	...
ρ_* (kg cm $^{-3}$)	\mathcal{N} (1600, 100)	1567^{+101}_{-100}
m_{dilution}	Fixed 1.0	...
m_{flux}	\mathcal{N} (0.0, 0.1)	$-0.000002^{+0.000012}_{-0.000012}$
σ_w (ppm)	\mathcal{J} (0.1, 1000.0)	949^{+22}_{-25}
T_0 (BJD)	\mathcal{N} (2458401.4, 0.5)	$2458401.4086^{+0.0032}_{-0.0032}$
T_1 (BJD)	\mathcal{N} (2458483.2, 0.5)	$2458483.2110^{+0.0034}_{-0.0034}$
T_2 (BJD)	\mathcal{N} (2458565.1, 0.5)	$2458565.0902^{+0.0032}_{-0.0033}$
T_3 (BJD)	\mathcal{N} (2458647.3, 0.5)	$2458647.3328^{+0.0043}_{-0.0045}$
T_8 (BJD)	\mathcal{N} (2459065.2, 0.5)	$2459065.2370^{+0.0024}_{-0.0023}$
T_9 (BJD)	\mathcal{N} (2459148.5, 0.5)	$2459148.4782^{+0.0027}_{-0.0026}$
T_{10} (BJD)	\mathcal{N} (2459231.1, 0.5)	$2459231.1144^{+0.0021}_{-0.0021}$
T_{11} (BJD)	\mathcal{N} (2459313.3, 0.5)	$2459313.2535^{+0.0019}_{-0.0019}$
T_{19} (BJD)	\mathcal{N} (2459976.1, 0.5)	$2459976.0493^{+0.0043}_{-0.0045}$
T_{20} (BJD)	\mathcal{N} (2460059.6, 0.5)	$2460059.6189^{+0.0023}_{-0.0023}$
T_{21} (BJD)	\mathcal{N} (2460142.6, 0.5)	$2460142.6048^{+0.0022}_{-0.0023}$
P (days)	...	$82.97213^{+0.00013}_{-0.00013}$
t_0 (BJD)	...	$2458400.3906^{+0.0016}_{-0.0016}$
a (au)	...	$0.3546^{+0.0073}_{-0.0077}$
R_p (R_{Jup})	...	0.99 ± 0.05
i (deg)	...	$89.69^{+0.02}_{-0.03}$

Note. P was computed as a slope and t_0 as an intercept of a least-squares fit to the transit times.

4.2. Spectroscopic Data Analysis

We performed a period search in the FEROS RVs and activity index data using a generalized Lomb–Scargle (GLS) periodogram (M. Zechmeister & M. Kürster 2009). Figure 5 shows a stacked GLS periodogram of the FEROS spectroscopic data of TOI-4504. We found significant RV periodicity with a period of 84 days, consistent with the detected quasiperiodic signal of TOI-4504 c. The semiamplitude of the 84 day signal in the FEROS data is $\sim 185 \text{ m s}^{-1}$, corresponding to a planetary mass of $\sim 3.5 M_{\text{Jup}}$, validating the planetary nature of TOI-4504 c.

After subtracting this period, no other significant signals were detected in the RV residuals, although we recorded a very large RV scatter of the order of $\sim 100 \text{ m s}^{-1}$. Keeping in mind the relatively low number of RV data and the prior knowledge of the complexity of the TOI-4504 system having at least three planets, two of them Jovian-mass and the third a short-period Neptune, the RV jitter could be attributed to unresolved planet signals.

The second panel of Figure 5 reveals a prominent peak at a period of 41.2 days, crossing the 10% false-alarm probability threshold. As we will demonstrate in our results, this signal is likely induced by the nontransiting giant TOI-4504 d. Moreover, subtracting this signal by simultaneously modeling it alongside the dominant 84 day period failed to account for the observed large RV scatter. As shown in Section 4.3, even a more sophisticated N -body modeling approach could not fully

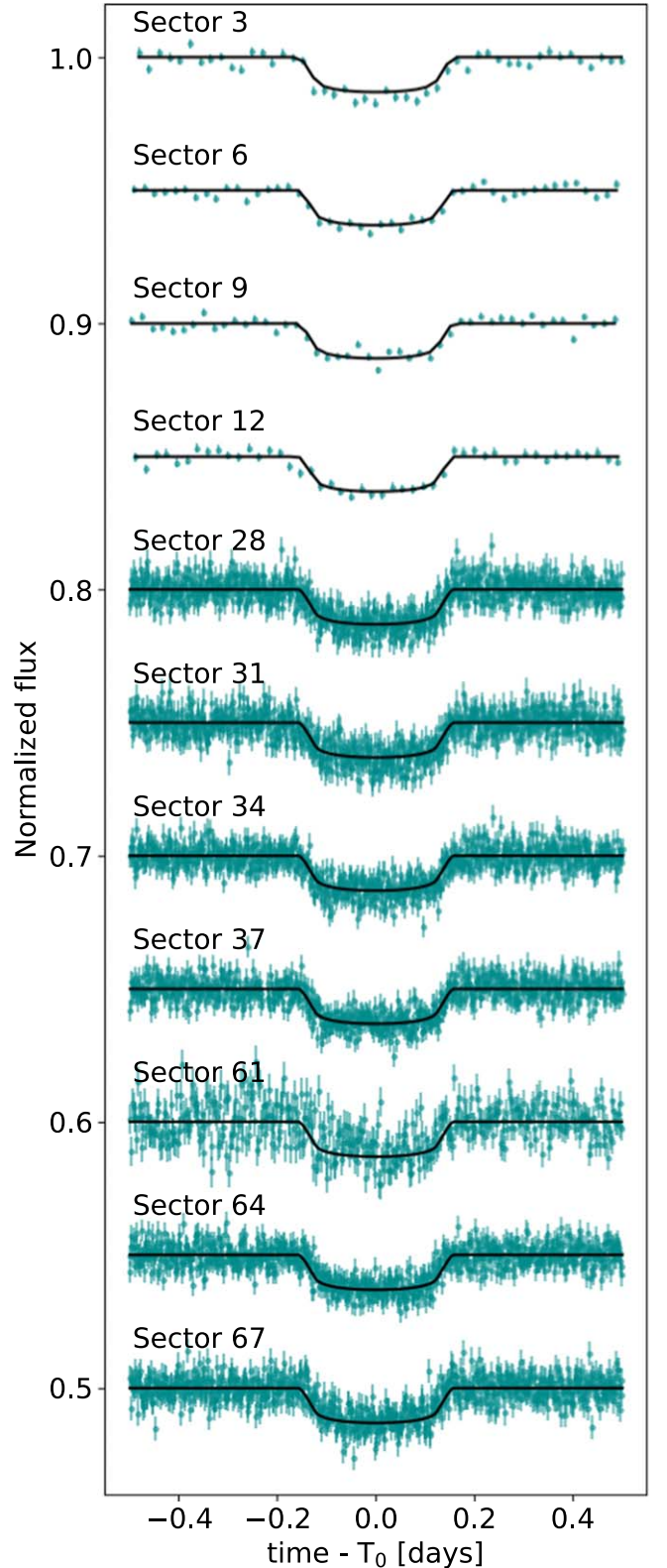


Figure 4. Transits of TOI-4504 c with a model from Juliet shifted to have midtransit at 0 and plotted with vertical offsets.

resolve the observed RV scatter. A GLS analysis of the N -body model RV residuals (see third panel of Figure 5) shows several peaks with periods of 2.33, 12.16, and 41.66 days; the latter is close to the osculating period of TOI-4504 d. However, all

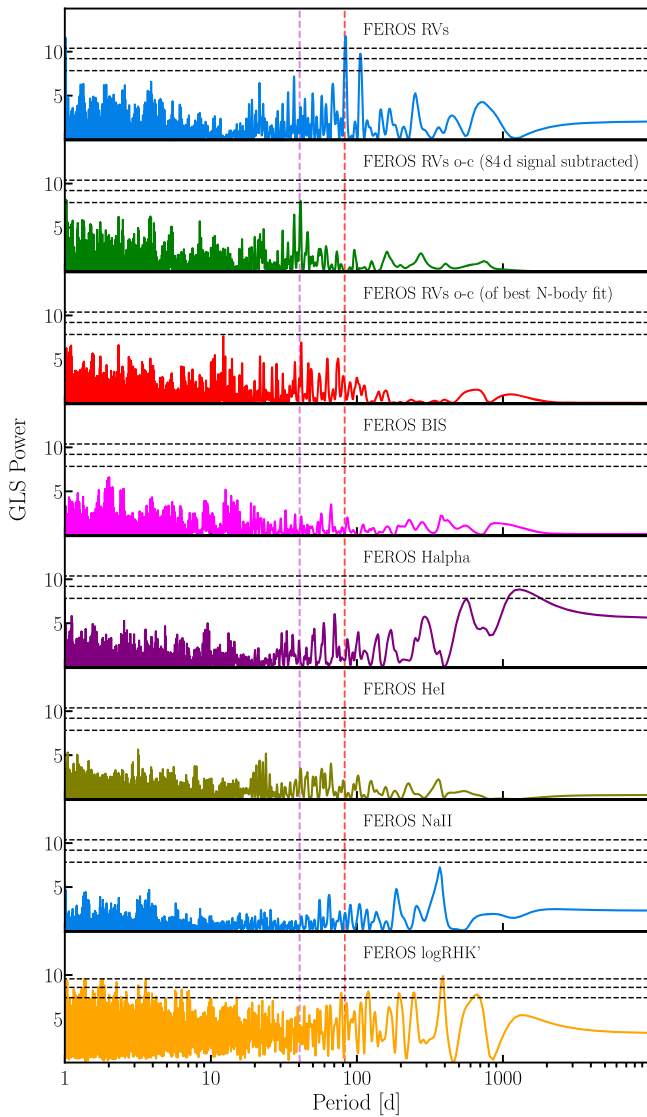


Figure 5. GLS power spectrum of FEROS spectroscopic products of TOI-4504. From top to bottom, as labeled, RVs used in this work, RV residuals after subtracting the dominant signal of TOI-4504 c at 84 days, the final best-fit TTV+RV model residuals, BIS, H_{α} , He I, Na II, and $\log(R'_{HK})$ activity indicators, respectively. False-alarm probability levels of 10%, 1%, and 0.1% are marked with dashed lines. The red and magenta vertical lines indicate the best-fit periods of the transiting Jovian planet TOI-4504 c and the nontransiting TOI-4504 d, respectively.

peaks are insignificant and likely emerged by chance, unrelated to planetary signals. We conclude that the precision of the RV data was sufficient to constrain the mass of TOI-4504 c, and, when constrained by TOI-4504 c, the TTV signal could constrain the period and mass of the nontransiting massive planet. However, the FEROS RVs were insufficient for constraining the parameters of the hot planet TOI-4504 b, which has an expected RV semiamplitude of only a few m s^{-1} .

The BIS, H_{α} , He I, and Na II did not show significant periodicity. However, it is worth mentioning that this is not the case for the $\log(R'_{HK})$ activity indicator, which showed many marginally significant periods, indicating that TOI-4504 is an active star, which may partially explain the large RV scatter. The large RV scatter in the FEROS data likely results from stellar activity, but we do not rule out additional planets in the system, an analysis of which is beyond the scope of this work.

4.3. Orbital Modeling Based on TTV and RV Data

In this section, we report the orbital analysis results of TOI-4504 c and its indirectly detected neighbor, which we call TOI-4504 d. We analyzed TOI-4504 c and d separately because, as we discussed in Section 4.2, we were not able to set constraints on the mass of the transiting planet TOI-4504 b with the FEROS RV data or with detailed three-planet N -body modeling of the TESS transits and TTVs separately or together with the RV data. We note in passing that we performed a three-planet orbital analysis including TOI-4504 b, but including TOI-4504 b did not significantly improve the fit compared to the models considering only TOI-4504 c and d and thus shall not be discussed in this work.

We conducted a joint global orbital analysis using broad priors to explore the parameter space consistent with the TTV and RV data for TOI-4504 using the Exo-Striker²⁷ exoplanet modeling toolbox (T. Trifonov 2019). Our fitting scheme followed a more targeted N -body orbital fit once the consistent parameter space had been identified. Taking the gravitational interactions between TOI-4504 c and d into account, the Exo-Striker uses an internal RV dynamical model, whereas the TTV model is wrapped around the TTVfast package (K. M. Deck et al. 2014). We follow a very similar TTV+RV N -body fitting approach, used by T. Trifonov et al. (2021) for the TOI-2202 system, which is similar to TOI-4504 in many aspects. We refer the reader to T. Trifonov et al. (2021) for more details, and below, we summarize our fitting methods, used parameters, adopted priors, and more results relevant to our modeling cascade, which reveal the orbital and physical parameters of the TOI-4504 c and d pair.

The fitted parameters for each planet in the TTV+RV model were the RV semiamplitude $K_{c,d}$ and the osculating planetary orbital period $P_{c,d}$. The eccentricities $e_{c,d}$, arguments of periastron $\omega_{c,d}$, and mean anomalies $M_{c,d}$ were derived using the parameterization $h = e \sin \omega$, $k = e \cos \omega$, and $\lambda = \omega + M$, which is more efficient for orbits with small eccentricities (X. Tan et al. 2013). Since we know that the perturber planet is not transiting, we assumed a non-coplanar, mutually inclined orbital geometry and fitted for the orbital inclinations $i_{c,d}$ and the difference between the longitudes of the ascending nodes $\Delta\Omega_{d-c} = \Omega_d - \Omega_c$, where the mutual inclination comes following the expression

$$\Delta i = \arccos[\cos(i_d)\cos(i_c) + \sin(i_d)\sin(i_c)\cos(\Delta\Omega)]. \quad (2)$$

Since only $\Delta\Omega$ is important, we kept Ω_d fixed to 0° , and we fit for Ω_c .

All osculating parameters in our N -body fitting were defined in the Jacobi coordinate system, which is standard practice for multiple-planet systems (M. Lee & S. Peale 2003), and are valid for the reference epoch BJD = 2458400.0, arbitrarily chosen before the first TESS transit of TOI-4504 c. Additionally, for the FEROS RV data, we fitted the RV offset and RV jitter parameters (see R. V. Baluev 2009). For the stellar mass of TOI-4504, we used $0.885 M_{\odot}$, which, together with the fitted parameters, was converted to the dynamical planetary masses $m_{c,d}$ needed to construct the N -body model. The numerical time step in the dynamical model was set to 0.5 day, which is sufficiently small for accurate modeling of the system.

We first used a global nested sampling (NS) parameter search (J. Skilling 2004) via the Dynesty sampler (J. S. Speagle 2020).

²⁷ Available at <https://github.com/3fon3fonov/exostriker>.

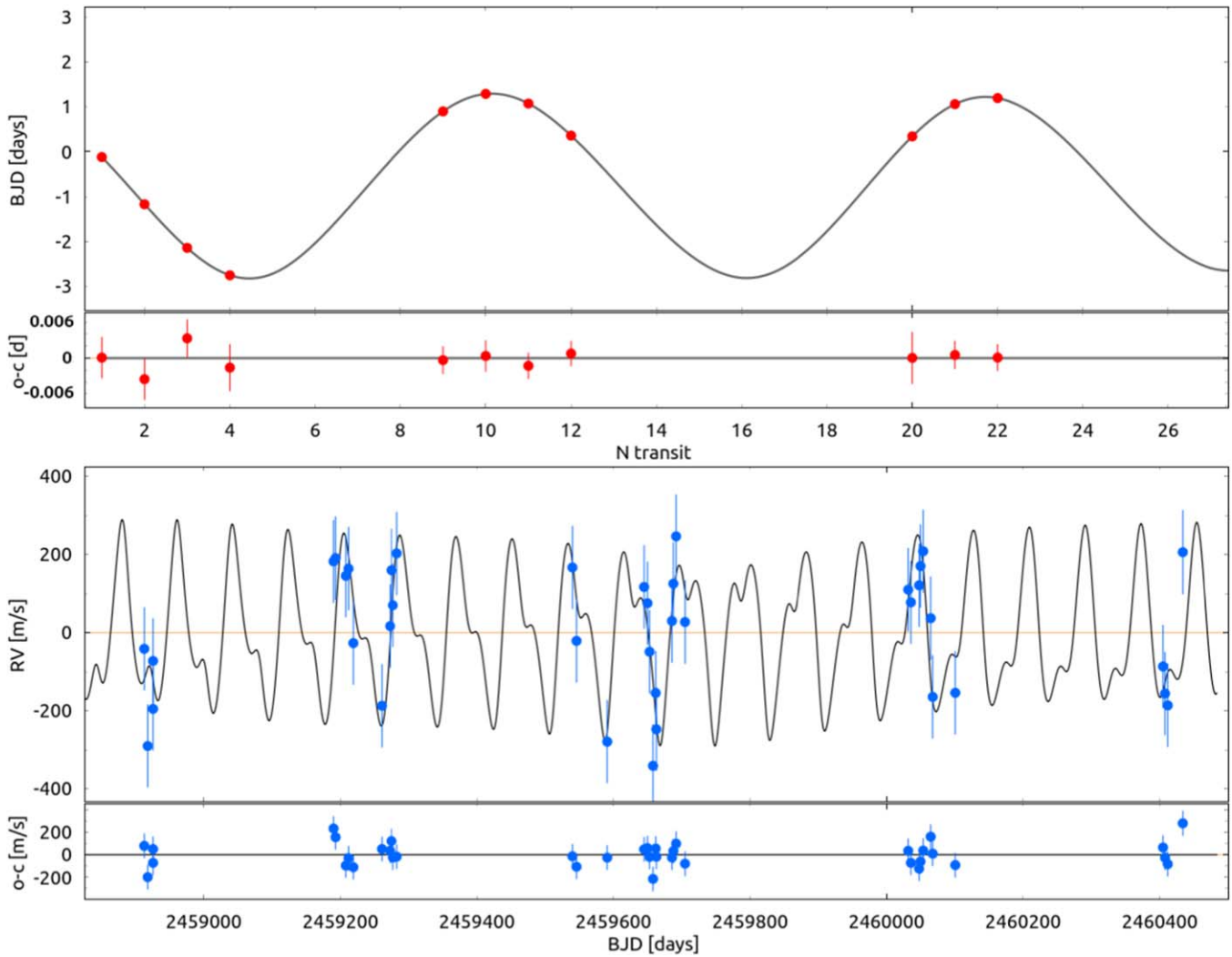


Figure 6. TESS TTV time series of TOI-4504 c and a model consistent with two Jovian-mass planets with periods close to the 2:1 MMR commensurability, with the nontransiting planet being interior (top panel). The TTV signal is expressed as the deviation of the TESS transit events with respect to the mean osculating period of TOI-4504 c, which has a large semiamplitude of ~ 2 days and a superperiod of 946.5 days. The bottom subpanel shows the TTV residuals. The main bottom panel shows the Doppler component of the same model fitted to the FEROS RV data. The bottom subpanel shows the RV residuals.

We employed a static NS setup with 500 “live points” per fitted parameter (see J. S. Speagle 2020 for details) to explore a wide parameter space of eccentricities, masses, and periods for the “yet-to-be-detected” planet TOI-4504 d, assuming it could be either interior or exterior to TOI-4504 c. For TOI-4504 c, the prior parameter range estimates were taken from our GLS and TTV extraction analysis, making the parameter search more constrained. The adopted prior ranges for TOI-4504 d and c are listed in Table A1. Our results showed very poor fits when TOI-4504 d was assumed to be exterior. In contrast, good fits were found in the resulting posterior probability distribution analysis when the planet was considered interior. As indicated in Figure A1, the posteriors are multimodal but firmly converge, with TOI-4504 d being an interior planet in the 2:1 period ratio commensurability.

As a next step, we used the NS posteriors and the best $-\ln \mathcal{L}$ NS solution as an initial guess for a more targeted simplex optimization (J. A. Nelder & R. Mead 1965), aiming to find the optimal $-\ln \mathcal{L}$ best-fit solution. This was followed by an affine-invariant ensemble Markov Chain Monte Carlo (MCMC) sampler (J. Goodman & J. Weare 2010) via the `emcee`

package (D. Foreman-Mackey et al. 2013) to build the parameter posteriors and obtain parameter uncertainties.

Figure 6 shows our best joint fit to the TTVs and RVs, whereas Figure A2 displays the MCMC posteriors drawn around the best fit. Table 4 lists the best fit in terms of the optimal $-\ln \mathcal{L}$ shown in Figure 6, the median orbital parameters and their uncertainties extracted from our MCMC posteriors, and the used priors. Figure 7 shows the phased RV planet signals of TOI-4504 c and d. The top two panels of Figure 7 show the phased planetary periods to the N -body fit, which, due to the dynamical nature of the model, are strongly osculating. In contrast, the bottom two panels provide a clearer representation of the RV signals, phased to the main osculation periods from the TTV+RV N -body model, which we estimate to be $82.5438^{+0.0150}_{-0.0176}$ days and $40.5634^{+0.0363}_{-0.0368}$ days for TOI-4504 c and d, respectively. We conclude that the TTVs from TESS and the RV data from FEROS suggest the presence of a massive pair of Jovian planets with osculating periods of $P_d = 40.5634^{+0.0365}_{-0.0368}$ days and $P_c = 82.5438^{+0.0176}_{-0.0150}$ days and small but significantly nonzero eccentricities of $e_d = 0.0445^{+0.0010}_{-0.0009}$ and $e_c = 0.0320^{+0.0016}_{-0.0014}$, valid for the reference epoch of BJD = 2458400.0. We obtain dynamical masses of $m_d = 1.417$

Table 4
MCMC Sampling Priors, Posteriors, and the Optimum $-\ln \mathcal{L}$ Orbital Parameters of the Two-planet System

Parameter	Median and 1σ Planet d	Max. $-\ln \mathcal{L}$		Adopted Priors		
		Planet c	Planet d	Planet c	Planet d	Planet c
K (m s $^{-1}$)	90.8366 $^{+1.8812}_{-2.5466}$	190.8921 $^{+4.7269}_{-6.2119}$	91.3360	189.2623	$\mathcal{U}(80.0, 140.0)$	$\mathcal{U}(150.0, 250.0)$
P (days)	40.5634 $^{+0.0363}_{-0.0368}$	82.5438 $^{+0.0150}_{-0.0176}$	40.5586	82.5383	$\mathcal{U}(40.2, 40.6)$	$\mathcal{U}(81.0, 83.0)$
$e \sin(\omega)$	0.0439 $^{+0.0010}_{-0.0011}$	-0.0320 $^{+0.0014}_{-0.0016}$	0.0441	-0.0320	$\mathcal{U}(-0.1, 0.1)$	$\mathcal{U}(-0.1, 0.1)$
$e \cos(\omega)$	-0.0064 $^{+0.0039}_{-0.0047}$	0.0005 $^{+0.0011}_{-0.0013}$	-0.0027	-0.0009	$\mathcal{U}(-0.1, 0.1)$	$\mathcal{U}(-0.1, 0.1)$
λ (deg)	9.89 $^{+3.45}_{-2.43}$	83.97 $^{+0.12}_{-0.15}$	14.11	83.80	$\mathcal{U}(0.0, 360.0)$	$\mathcal{U}(70.0, 110.0)$
i (deg)	85.00 $^{+0.28}_{-0.30}$	89.69 $^{+0.03}_{-0.03}$	84.74	89.68	$\mathcal{N}(86.0, 3.0)$	$\mathcal{N}(89.7, 0.1)$
$\Delta\Omega$ (deg)	...	0.0 $^{+0.9}_{-1.0}$...	-0.8	...	$\mathcal{N}(0.0, 30.0)$
RV _{off} FEROS (m s $^{-1}$)	...	2067.0517 $^{+14.2161}_{-14.8783}$...	2064.9642	...	$\mathcal{U}(1900.0, 2200.0)$
RV _{jit} FEROS (m s $^{-1}$)	...	103.3721 $^{+13.8367}_{-7.0042}$...	104.6664	...	$\mathcal{U}(1.0, 150.0)$
e	0.0445 $^{+0.0010}_{-0.0009}$	0.0320 $^{+0.0016}_{-0.0014}$	0.0441	0.0320	(derived)	(derived)
ω (deg)	98.3 $^{+6.1}_{-5.1}$	270.9 $^{+2.0}_{-2.2}$	93.5	268.4	(derived)	(derived)
M_0 (deg)	271.6 $^{+7.3}_{-7.5}$	173.1 $^{+2.1}_{-1.9}$	280.6	175.4	(derived)	(derived)
Δi (deg)	...	4.7 $^{+0.3}_{-0.3}$...	5.0	...	(derived)
m_p (M_{Jup})	1.4166 $^{+0.0651}_{-0.0647}$	3.7672 $^{+0.1810}_{-0.1822}$	1.4294	3.7494	(derived)	(derived)
a_p (au)	0.2219 $^{+0.0041}_{-0.0043}$	0.3569 $^{+0.0066}_{-0.0069}$	0.2219	0.3569	(derived)	(derived)

Note. Derived by joint N -body modeling of TTVs (TESS) and RVs (FEROS). The orbital elements are in the Jacobi frame and are valid for epoch BJD = 2458400.0. The adopted priors are listed in the right-most columns, and their meanings are \mathcal{U} : uniform and \mathcal{N} : Gaussian priors. The derived planetary posterior parameters of a and m are calculated by considering the stellar parameter uncertainties.

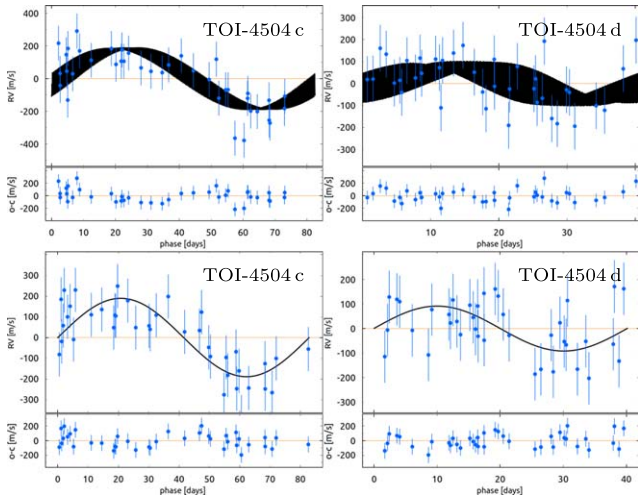


Figure 7. Phased RV signals for the planets TOI-4504 c and d. The top two panels display the planetary signals along with the osculating N -body model, phased to the best-fit periods from Table 4, valid for BJD = 2458400.0. The bottom two panels illustrate the same planetary signals, phased to the mean osculation periods derived from the TTV+RV model.

$^{+0.065}_{-0.065} M_{\text{Jup}}$ and $m_c = 3.767^{+0.182}_{-0.181} M_{\text{Jup}}$ for TOI-4504 d and TOI-4504 c, respectively. The mutual inclination between the two planets suggests a non-coplanar configuration with $\Delta i = 4.7^{+0.3}_{-0.3}^\circ$, which agrees with the fact that TOI-4504 d is not transiting.

4.4. Dynamics and Long-term Stability

We performed N -body simulations to study the long-term stability and dynamical evolution of the TOI-4504 system. For this test, we again ignored the innermost planet, TOI-4504 b, since, even if its dynamical mass is in the Neptune-mass regime, its overall mutual Hill distance with TOI-4504 d would be $\sim 17 R_{\text{Hill},m}$ (see B. Gladman 1993) and thus would result in minimal dynamical interactions with the outer pair.

Additionally, including TOI-4504 b would require using a very small time step of approximately 30 minutes (1/100 of the orbital period of the planet) to achieve accurate orbital dynamics, which would be computationally expensive.

Our study of the long-term dynamics and possible MMR dynamics in the system adopted the same N -body numerical setup used in our recent analyses of the TOI-2202 (T. Trifonov et al. 2021) and TOI-2525 (T. Trifonov et al. 2023) systems, which share similar physical and orbital characteristics with the Jovian pair of TOI-4504. We conducted numerical integrations using a custom version of the Wisdom–Holman N -body integrator (J. Wisdom & M. Holman 1991), specifically tailored for long-term stability analyses of exoplanetary systems in Jacobi orbital elements. Integrated natively within the Exo-Striker toolbox, this N -body integrator allows direct injection of posterior samples in Jacobi coordinates, thereby avoiding the additional coordinate transformations typically required by other publicly available N -body integrators. We tested the stability of the TOI-4504 system for a maximum of 10 million yr with a time step of 0.5 day for 10,000 randomly chosen samples from the achieved orbital parameters of the TTV+RV MCMC parameter posteriors. For each sample integration and at each numerical time step, we monitor the planetary semimajor axes, ensuring that they do not deviate by more than 20% from their initial values; any orbit exceeding this threshold is considered unstable, resulting in the termination of the integration. Additionally, integrations are flagged as unstable and terminated if eccentricity values become sufficiently excited to orbit-crossing configurations. Further details on our stability criteria are provided in T. Trifonov et al. (2021).

We found that all examined parameters are long-term stable. From the numerical evolution, we built a posterior distribution of some of the important dynamical properties of the system, such as the mean period ratio P_{rat} , mean eccentricities \hat{e}_d , \hat{e}_c , their peak-to-peak amplitudes e_d , e_c , the dynamical masses of the planets m_d , m_c , and the orbital semimajor axes a_d , a_c , as in

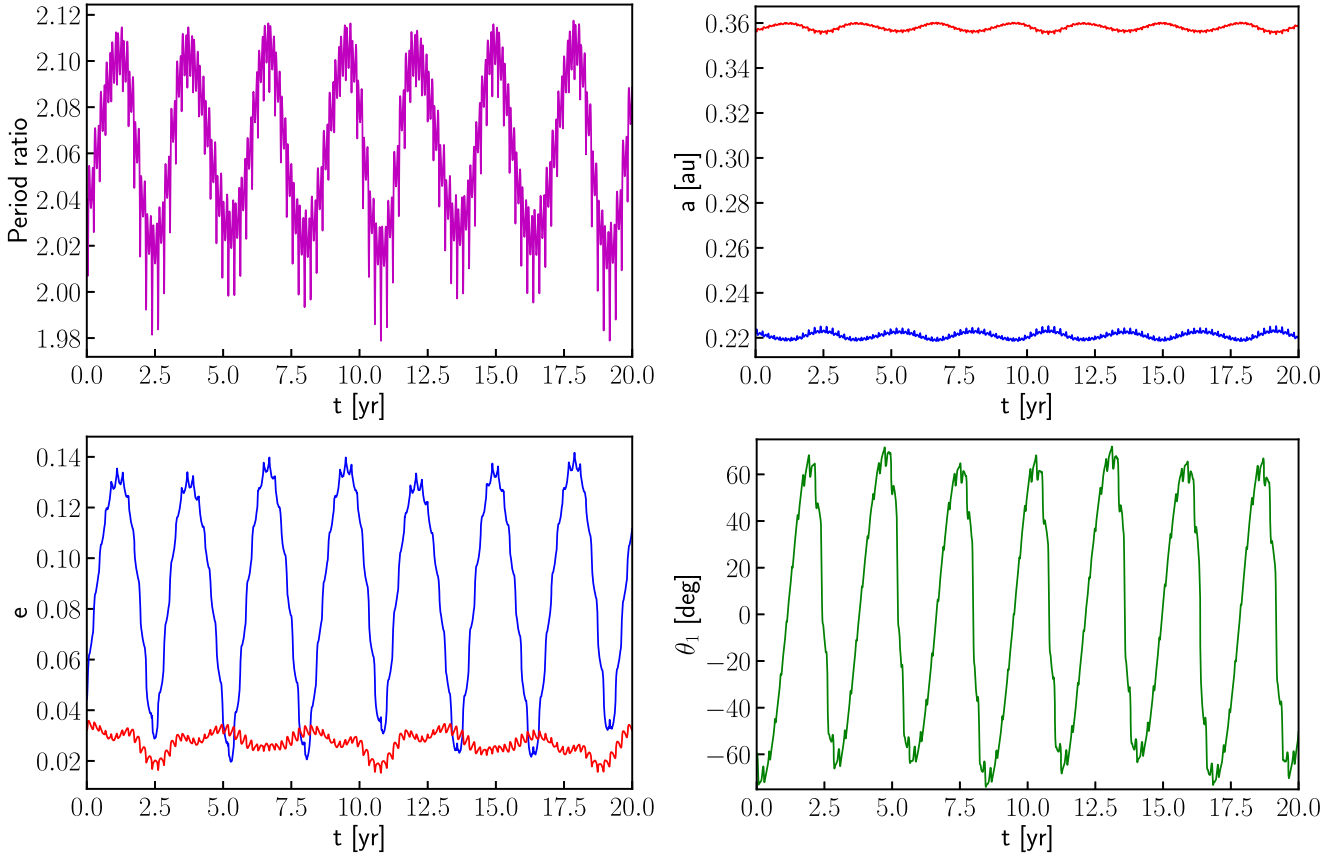


Figure 8. Orbital evolution of the best TTV+RV N -body model of the TOI-4504 system for a short extent of 20 yr long N -body simulation using the Exo-Striker. The top row from left to right panels shows the evolution of the planetary period ratio (P_c/P_d) (magenta) and the evolution of the semimajor axes a_c (red) and a_d (blue). The bottom row from left to right panels shows the evolution of the eccentricities e_c (red) and e_d (blue) and θ_1 (green), which librates around 0° with an amplitude of $\sim 65^\circ$.

T. Trifonov et al. (2021, 2023). We also collected posterior distributions of the resonance angles, defined as

$$\Delta\omega = \omega_c - \omega_d, \quad (3)$$

which is the secular apsidal angle, and

$$\theta_1 = \lambda_c - 2\lambda_d + \omega_c \quad \text{and} \quad \theta_2 = \lambda_c - 2\lambda_d + \omega_d \quad (4)$$

are the first-order eccentricity-type 2:1 MMR angles, of which at least one must librate around a fixed angle to claim the system in an MMR (see M. H. Lee 2004).

We find that the TOI-4504 system exhibits moderate eccentricity evolution, with the less massive planet, TOI-4504 d, showing larger eccentricity variations, from 0.02 to 0.12. In all cases, the period ratio oscillates around ~ 2.06 , slightly above the exact 2:1 period ratio. The angles θ_2 and $\Delta\omega$ circulate between 0° and 360° , while θ_1 librates around 0° with a mean semiamplitude of 73° for all integrated samples. This libration of θ_1 in all samples implies that the massive planets in the TOI-4504 system are involved in a 2:1 MMR, despite the minor offset in period ratio, which, given the strong dynamical interactions, is needed to maintain the resonance.

Figure 8 shows an example of a 20 yr extent of the orbital evolution simulation started from the best fit (i.e., maximum $-\ln\mathcal{L}$; see Table 4). We show the evolution of the mutual period ratio P_{rat} , the eccentricities e_c and e_d , and the first-order eccentricity-type 2:1 MMR angle θ_1 . The evolution of the model based on the best-fit parameters is indicative of the

orbital evolution of the posterior samples. The libration of θ_1 is sufficient to conclude that the TOI-4504 Jovian pair is involved in a 2:1 MMR (M. H. Lee 2004).

4.5. Internal Composition of TOI-4504 c

For TOI-4504 c, we computed planet interior models and their thermal evolution with MESA (B. Paxton et al. 2011, 2013), following the implementation described in M. I. Jones et al. (2024). In this case, we modeled the planet with the heavy elements condensed in an inert isodensity core surrounded by a pure gas (H/He) envelope. We assumed a 1:1 mixture of rock and ice for the core, with their density obtained from the ρ - P relations presented in W. B. Hubbard & M. S. Marley (1989). The density of the mixture was computed using the additive volume law. We evolved different models with different masses of the core and compared them with the current position of TOI-4504 c in the radius–age diagram. Figure 9 shows different models that agree at the 1σ level with the current radius of the planet. These results correspond to a planet metallicity of $Z_p = 0.21^{+0.07}_{-0.09}$ and a corresponding heavy-element enrichment with respect to the host star of $Z_p/Z_\star = 9.6^{+3.1}_{-4.1}$.

5. Summary and Conclusions

In this work, we report the discovery and orbital analysis of a multiplanetary system orbiting the K dwarf star TOI-4504. We analyzed available photometric data from TESS and conducted follow-up spectroscopic observations with FEROS to constrain

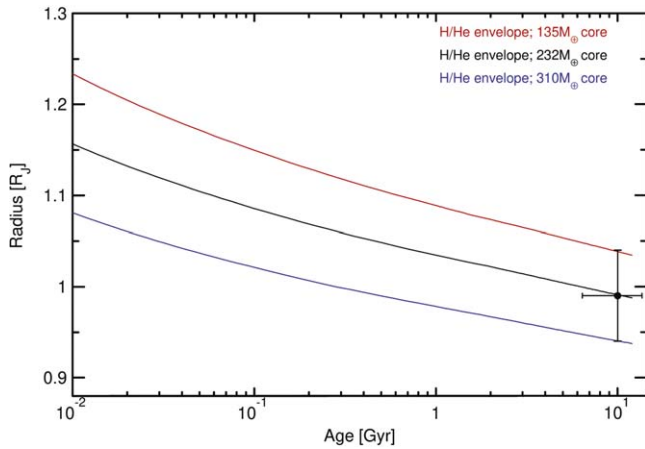


Figure 9. Position of TOI-4504 c in the age–radius diagram (black dot). Three different models with an isodensity core ($\rho = 15 \text{ g cm}^{-3}$) with different masses and surrounded by a H/He envelope are overplotted (solid lines).

the orbital and physical parameters of the detected exoplanets. We confirm two transiting planets, TOI-4504 b and TOI-4504 c, and we discover an additional Jovian-mass exoplanet, TOI-4504 d, based on the dynamical perturbations induced on TOI-4504 c, evidenced by strong TTVs with the largest ever detected semi-amplitude of ~ 2 days. Our analysis indicates that the TOI-4504 system consists of a hot sub-Neptune and two warm Jovian planets in a 2:1 MMR.

The innermost planet, TOI-4504 b, was only detected in the TESS photometry with a period of $2.42614^{+0.00014}_{-0.00013}$ days and an estimated radius of $2.69 \pm 0.19 R_{\oplus}$. The precision of our RVs is not enough to measure the mass of this potential $\sim 10 M_{\oplus}$ sub-Neptune (S. Müller et al. 2024). TOI-4504 b is a potentially interesting candidate for further characterization of its possible atmospheric composition with JWST (e.g., N. Madhusudhan et al. 2023; M. Holmberg & N. Madhusudhan 2024). TOI-4504 b has a predicted transmission spectroscopy metric of ~ 20 (E. M. R. Kempton et al. 2018) and is among the handful of hot sub-Neptunes transiting solar-type stars that can be observed with NIRSpec/Prism avoiding saturation, which allows for obtaining a transmission spectrum with wide wavelength coverage ($0.6\text{--}5.3 \mu\text{m}$) from a single transit.

TOI-4504 c was detected in the TESS data and FEROS RVs and has a period of $82.5438^{+0.0150}_{-0.0176}$ days valid for epoch BJD = 2458400, a mean orbital period of $82.8540^{+0.0009}_{-0.0010}$ days, an estimated radius of $0.9897 \pm 0.0092 R_{\text{Jup}}$, and a dynamical mass estimate of $3.7672^{+0.1810}_{-0.1822} M_{\text{Jup}}$. TOI-4504 c exhibits very large TTVs with a superperiod of ~ 2.9 yr and a peak-to-peak amplitude of ~ 4 days.

Our orbital analysis was focused only on the TTV+RV data for TOI-4504 c and its nontransiting perturbing planet, TOI-4504 d. Using a self-consistent TTV+RV model scheme coupled with various optimization and sampling techniques, we were able to pinpoint TOI-4504 d's period to be $40.5634^{+0.0363}_{-0.0368}$ days valid for epoch BJD = 2458400, a mean orbital period of $40.1716^{+0.0145}_{-0.0158}$ days, and a dynamical mass of $1.4166^{+0.0651}_{-0.0647} M_{\text{Jup}}$.

TESS has already found several strong TTV systems around relatively bright stars, which were effectively followed with ground-based spectroscopic facilities to measure their masses in conjunction with their TTV signals. Combining precise RV and TTV data allows for a refined determination of the

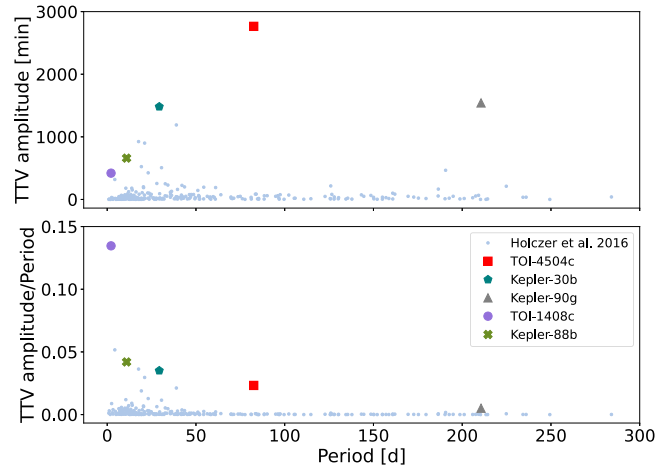


Figure 10. TOI-4504 c in context of other planets with significant TTVs, and planets from T. Holczer et al. (2016) in period-TTV amplitude and period-TTV amplitude and period ratio diagram. TTV amplitude is a peak-to-node amplitude of sinus fit, for Kepler-90 g it is the maximum observed difference between the time lapsed between consecutive transits.

planetary masses and the system's geometry and dynamical state, aiding in understanding their formation and evolution. One of these systems is TOI-216 (R. I. Dawson et al. 2019, 2021). This system hosts a pair of warm gas giants librating at the 2:1 MMR. Another pair of warm giant planets close to 2:1 resonance orbit K-type star TOI-2202 (T. Trifonov et al. 2021). TOI-2202 is a K-type star that also hosts a pair of warm giants near the 2:1 MMR. (T. Trifonov et al. 2023). TESS observed just a single transit in TIC 279401253, but follow-up RV data are well fit by a pair of eccentric super-Jupiters in the 2:1 resonance, which would imply large TTVs (V. Bozhilov et al. 2023). However, in some respects, the TOI-4504 system shares most similarities with the nontransiting nearby M dwarf system GJ 876, which was discovered by RVs (E. J. Rivera et al. 2005; S. Millholland et al. 2018). GJ 876 hosts a hot super-Earth planet and three other planets trapped in 1:2:4 MMR, a pair of gas giants (in 2:1 MMR), with the outer planet in the chain being Neptune-mass.

In the context of the GJ 876 system, the massive resonant pairs in TOI-4504 and GJ 876 likely reached their current orbits via slow, convergent type II migration combined with planet–planet interactions (see, e.g., M. H. Lee & S. J. Peale 2002; W. Kley & R. P. Nelson 2012). Similar to systems such as TOI-216, TOI-2202, TOI-2525, and particularly GJ 876, the TOI-4504 system supports the planet formation and subsequent migration theories, which effectively explain the observed MMR geometries of massive exoplanets.

T. Holczer et al. (2016) made a transit timing catalog of Kepler objects of interest (KOIs) and sorted out several KOIs that showed significant TTVs with long-term variations (see Table 5 in T. Holczer et al. 2016). Figure 10 shows TOI-4504 c in context with other planets with significant TTVs. As can be seen from the top panel of Figure 10, the peak-to-node amplitude of the TTVs of TOI-4504 c is about twice as big as that of Kepler-30 b, a planet with the largest previously known TTV semi-amplitude (F. Panichi et al. 2018). However, when calculating the relative amplitude of the TTV with respect to the orbital period of the planet, TOI-4504 c is not the record holder, although it still belongs to a small group of planets with large relative TTVs (the bottom panel of Figure 10).

The planet with the largest known TTVs relative to its orbital period is TOI-1408 c, a sub-Neptune on a very short orbital period (J. Korth et al. 2024). Our dynamical solution implies that an observer located such that planet d was observed to transit (which is more than 1.6 times as likely as our view of planet c transiting) would observe TTVs more than 50% larger than those that TESS observed for planet c. Thus, the ratio of d's TTVs to its orbital period would be almost as large as those of hot sub-Neptune TOI-1408 c (J. Korth et al. 2024).

Additional observations are needed to explain the large RV jitter observed in TOI-4504 and refine the orbital and physical parameters of the system. Although our fit to the TTVs is very good, additional observations are needed to further refine the orbital architecture of the TOI-4504 c and d pair. Transits of TOI-4504 c numbers 29 and 31 (Table A2) will be observed by TESS in sectors 89 and 95, respectively. Due to significant uncertainties in the predicted transits, ground-based observations will be difficult. Observing campaigns on the nights around the predicted transits would be appreciated. TOI-4504 is within the southern PLATO field and should be monitored continuously for 2 yr beginning in 2027 (transits 38 and further).

Since our RV model could not fully resolve the large RV scatter around the fit, the source of the RV jitter remains unclear. The current RV data conclusively confirm the presence of two resonant planets. However, more precise RV measurements are needed to determine the mass of the innermost planet, further constrain the orbital parameters and eccentricities of TOI-4504 d and TOI-4504 c, and eventually reveal the presence of additional planets in the system.

Since TOI-4504 is a rather faint target for the 2.2 m telescope with FEROS at La Silla, more precise RVs are urgently needed with facilities like ESPRESSO (F. Pepe et al. 2021) to measure the planetary masses and eccentricities more accurately. We plan to continue our monitoring of TOI-4504 with transit and RV measurements, which will allow us to extend our orbital analysis, capturing the gravitational effects of the planets across the full transit light curve using a photodynamical model. These models can measure transit depths and durations, thereby better constraining the dynamic state of the system and shedding more light on the system's origin and migration processes.

Acknowledgments

We thank the anonymous referee for comments that helped to improve the manuscript. M.V., M.S., and P.K. acknowledge support by Inter-transfer grant No. LTT-20015. M.V. also acknowledges a travel subsidy from grants ANID-23-05 and EU MSCA EXOWORLD project ID:101086149. R.B. acknowledges support from FONDECYT project 1241963 and from ANID—Millennium Science Initiative—ICN12_009. T.T. acknowledges support by the BNSF program “VIHREN-2021” project No. KP-06-DV/5. M.T.P. acknowledges the support of Fondecyt-ANID fellowship No. 3210253 and ANID ASTRON-0037 project. A.J. acknowledges support from ANID—Millennium Science Initiative—ICN12_009 and AIM23-0001 and FONDECYT project 1210718. K.A.C. acknowledges support from the TESS mission via subaward s3449 from MIT. This work was funded by the Data Observatory Foundation. This work was funded by ANID Vinculación Internacional FOVI220091. This research has made use of the Exoplanet Follow-up Observation Program (ExoFOP; doi:10.26134/ExoFOP5) website, which is operated by the California Institute of Technology, under contract with

the National Aeronautics and Space Administration under the Exoplanet Exploration Program. Funding for the TESS mission is provided by NASA's Science Mission Directorate. We acknowledge the use of public TESS data from pipelines at the TESS Science Office and at the TESS Science Processing Operations Center. This paper includes data collected by the TESS mission that are publicly available from the Mikulski Archive for Space Telescopes (MAST). The specific observations analyzed can be accessed via doi:10.17909/g52w-sk09. STScI is operated by the Association of Universities for Research in Astronomy, Inc., under NASA contract NAS5-26555. Support to MAST for these data is provided by the NASA Office of Space Science via grant NAG5-7584 and by other grants and contracts. The results reported herein benefited from collaborations and/or information exchange within NASA's Nexus for Exoplanet System Science (NExSS) research coordination network sponsored by NASA's Science Mission Directorate under agreement No. 80NSSC21K0593 for the program “Alien Earths.” Resources supporting this work were provided by the NASA High-End Computing (HEC) Program through the NASA Advanced Supercomputing (NAS) Division at Ames Research Center for the production of the SPOC data products.

Facility: TESS, Max Planck:2.2m.

Software: Exo-Striker (T. Trifonov 2019), Juliet (N. Espinoza et al. 2019), Ceres (R. Brahm et al. 2017a), ZASPE (R. Brahm et al. 2017b), Tesseract (F. Rojas et al. 2024, in preparation), TESSCut (C. E. Brasseur et al. 2019), Lightcurve (Lightcurve Collaboration et al. 2018), Dynesty (J. S. Speagle 2020), Batman (L. Kreidberg 2015), Celerite (D. Foreman-Mackey et al. 2017).

Appendix Upcoming Transits of TOI-4504 c

In this Appendix, we show in Table A1 priors for the global NS run; in Table A2, we list the estimated midtransit time estimates of TOI-4504 c; in Table A3, we show RVs and activity indicators obtained with FEROS. Figure A1 shows the posterior distribution from a global joint TTV+RV static nested sampling search. In Figure A2, we show the posterior distribution from a focused joint TTV+RV MCMC sampling.

The N -body simulation, together with the best-fit solution of TTV+RV analysis, allowed us to predict future transit times of TOI-4504 c more than 10 yr in advance (Table A2). For completeness, we also give past transits since t_0 in Table A2.

Table A1

Priors for the Global NS Run, which Aimed to Identify the Parameter Space of TOI-4504 d Consistent with the TTVs of TOI-4504 c and RVs of TOI-4504

Parameter	Planet d	Planet c
K (m s^{-1})	$\mathcal{U}(30.0, 120.0)$	$\mathcal{U}(100.0, 250.0)$
P (days)	$\mathcal{U}(20.0, 60.0)$ and $\mathcal{U}(120.0, 300.0)$	$\mathcal{U}(81.0, 83.0)$
$e \sin(\omega)$	$\mathcal{U}(-0.10, 0.10)$	$\mathcal{U}(-0.10, 0.10)$
$e \cos(\omega)$	$\mathcal{U}(-0.10, 0.10)$	$\mathcal{U}(-0.10, 0.10)$
λ (deg)	$\mathcal{U}(-180.0, 360.0)$	$\mathcal{U}(70.0, 110.0)$
i (deg)	$\mathcal{N}(86.0, 3.0)$	$\mathcal{U}(89.7, 0.1)$
Ω (deg)	0 (fixed)	$\mathcal{N}(0.0, 30.0)$
RV off _{FEROS} (m s^{-1})	$\mathcal{U}(1950.0, 2150.0)$	
RV jit _{FEROS} (m s^{-1})	$\mathcal{U}(0.0, 150.0)$	

Table A2
Predicted Midtransit Times for TOI-4504 c

No.	BJD	No.	BJD	No.	BJD	No.	BJD
1	2458401.4086 ^{+0.0004} _{-0.0005}	21	2460059.6184 ^{+0.3886} _{-0.4373}	41	2461715.7660 ^{+1.0841} _{-1.2393}	61	2463371.0909 ^{+0.7731} _{-0.9278}
2	2458483.2231 ^{+0.0148} _{-0.0153}	22	2460142.5931 ^{+0.2823} _{-0.3086}	42	2461799.5893 ^{+1.0956} _{-1.2186}	62	2463454.1663 ^{+1.1786} _{-1.4180}
3	2458565.1073 ^{+0.0261} _{-0.0265}	23	2460224.9812 ^{+0.1716} _{-0.1876}	43	2461883.1822 ^{+0.9626} _{-1.0472}	63	2463537.7434 ^{+1.5151} _{-1.7736}
4	2458647.3635 ^{+0.0390} _{-0.0406}	24	2460306.9802 ^{+0.1116} _{-0.1171}	44	2461966.2880 ^{+0.6963} _{-0.7521}	64	2463621.5822 ^{+1.6493} _{-1.8876}
5	2458730.2564 ^{+0.0804} _{-0.0845}	25	2460388.8415 ^{+0.1139} _{-0.1206}	45	2462048.8016 ^{+0.4084} _{-0.4377}	65	2463705.3773 ^{+1.5622} _{-1.7615}
6	2458813.7926 ^{+0.1328} _{-0.1493}	26	2460470.8214 ^{+0.1758} _{-0.2082}	46	2462130.8606 ^{+0.2417} _{-0.2422}	66	2463788.8495 ^{+1.3020} _{-1.4355}
7	2458897.6602 ^{+0.1770} _{-0.1985}	27	2460553.1805 ^{+0.3396} _{-0.3916}	47	2462212.7309 ^{+0.1999} _{-0.2153}	67	2463871.8038 ^{+0.9202} _{-0.9814}
8	2458981.5652 ^{+0.2063} _{-0.2339}	28	2460636.1081 ^{+0.5527} _{-0.6330}	48	2462294.6947 ^{+0.2820} _{-0.3225}	68	2463954.2377 ^{+0.5587} _{-0.6102}
9	2459065.2622 ^{+0.2083} _{-0.2350}	29	2460719.5920 ^{+0.7512} _{-0.8437}	49	2462377.0283 ^{+0.5114} _{-0.5883}	69	2464036.3360 ^{+0.3851} _{-0.4052}
10	2459148.4917 ^{+0.1722} _{-0.1932}	30	2460803.4249 ^{+0.8599} _{-0.9630}	50	2462459.9463 ^{+0.8540} _{-0.9861}	70	2464118.3598 ^{+0.3946} _{-0.4653}
11	2459231.1206 ^{+0.1187} _{-0.1300}	31	2460887.3192 ^{+0.8721} _{-0.9664}	51	2462543.4456 ^{+1.1507} _{-1.3014}	71	2464200.5739 ^{+0.5998} _{-0.7364}
12	2459313.2552 ^{+0.0690} _{-0.0768}	32	2460970.9786 ^{+0.7765} _{-0.8496}	52	2462627.2792 ^{+1.2986} _{-1.4381}	72	2464283.1879 ^{+1.0083} _{-1.2111}
13	2459395.1287 ^{+0.0510} _{-0.0530}	33	2461054.1342 ^{+0.5618} _{-0.6253}	53	2462711.1361 ^{+1.2869} _{-1.4059}	73	2464366.2819 ^{+1.4592} _{-1.7046}
14	2459476.9771 ^{+0.0582} _{-0.0608}	34	2461136.6787 ^{+0.3407} _{-0.3664}	54	2462794.7524 ^{+1.1275} _{-1.2161}	74	2464449.7853 ^{+1.8135} _{-2.1040}
15	2459559.0306 ^{+0.0975} _{-0.1041}	35	2461218.7611 ^{+0.2007} _{-0.2035}	55	2462877.9109 ^{+0.8377} _{-0.8877}	75	2464533.5273 ^{+2.0046} _{-2.2332}
16	2459641.5272 ^{+0.1779} _{-0.1941}	36	2461300.6731 ^{+0.1820} _{-0.1945}	56	2462960.5230 ^{+0.5304} _{-0.5423}	76	2464617.2672 ^{+1.9669} _{-2.1452}
17	2459724.6306 ^{+0.2897} _{-0.3385}	37	2461382.7407 ^{+0.2812} _{-0.3265}	57	2463042.6845 ^{+0.3270} _{-0.3300}	77	2464700.7314 ^{+1.6552} _{-1.7739}
18	2459808.2733 ^{+0.3962} _{-0.4565}	38	2461465.2669 ^{+0.5158} _{-0.6066}	58	2463124.5967 ^{+0.2358} _{-0.2574}	78	2464783.7092 ^{+1.1508} _{-1.2096}
19	2459892.1846 ^{+0.4561} _{-0.5243}	39	2461548.3851 ^{+0.7916} _{-0.9165}	59	2463206.4837 ^{+0.2714} _{-0.3098}	79	2464866.1730 ^{+0.6756} _{-0.7025}
20	2459976.0671 ^{+0.4589} _{-0.5178}	40	2461631.9600 ^{+0.9770} _{-1.1403}	60	2463288.5747 ^{+0.4398} _{-0.5271}	80	2464948.2903 ^{+0.4509} _{-0.4299}

Note. No. gives the number of the transit since t_0 , and BJD gives the midtransit time.

Table A3
RV and Activity Indices of TOI-4504 Measured with FEROS

BJD	RV (m s ⁻¹)	Bisector	FWHM	SNR	H _α	log(<i>R</i> _{HK})	Na II	He I
2458912.730428	2023.5 ± 10.1	-48 ± 15	9.9507	49	0.1554 ± 0.004	-4.4426 ± 0.0641	0.2966 ± 0.0073	0.5121 ± 0.0097
2458917.7301462	1774.9 ± 11.7	-39 ± 17	9.9237	41	0.1346 ± 0.0043	-5.4889 ± 0.6482	0.3188 ± 0.0086	0.5219 ± 0.011
2458925.5538544	1992.5 ± 26.5	75 ± 34	10.0707	17	0.2872 ± 0.023	-4.1016 ± 0.0692	0.5544 ± 0.0441	0.6636 ± 0.0436
2458925.5970903	1869.9 ± 11.3	-66 ± 16	9.9409	42	0.1503 ± 0.0045	-4.9067 ± 0.1358	0.2471 ± 0.0076	0.536 ± 0.0106
2459189.7431016	2247.1 ± 10	-46 ± 15	9.8113	47	0.1494 ± 0.0042	-5.2786 ± 0.1929	0.2439 ± 0.0069	0.5176 ± 0.01
2459192.7143168	2255.4 ± 14.5	-79 ± 20	9.7936	32	0.1557 ± 0.0073	-4.706 ± 0.1078	0.2373 ± 0.0124	0.4613 ± 0.0152
2459207.7670343	2210.2 ± 10.6	-4 ± 15	9.8256	45	0.1463 ± 0.0043	-5.0808 ± 0.1269	0.1944 ± 0.0069	0.5163 ± 0.0102
2459211.7211734	2228.6 ± 10.9	21 ± 16	9.8664	44	0.1596 ± 0.0047	-5.0505 ± 0.1226	0.2142 ± 0.0073	0.5216 ± 0.0104
2459218.7262622	2038.1 ± 10	-47 ± 15	9.8061	49	0.1296 ± 0.0036	-4.9215 ± 0.1023	0.2176 ± 0.0061	0.5052 ± 0.0088
2459260.6382415	1877.8 ± 12	-14 ± 17	9.8243	39	0.1857 ± 0.0058	-5.2035 ± 0.2064	0.2347 ± 0.0086	0.513 ± 0.0116
2459272.776905	2081.6 ± 13.4	4 ± 19	9.8138	35	0.1369 ± 0.0055	-4.5168 ± 0.0767	0.2836 ± 0.0105	0.5342 ± 0.0138
2459274.716173	2224.5 ± 10.6	-1 ± 15	9.7323	45	0.1372 ± 0.0042	-5.4107 ± 0.3654	0.266 ± 0.0074	0.5071 ± 0.0097
2459276.7156498	2134.9 ± 12.9	-46 ± 18	10.0024	36	0.1444 ± 0.0048	-999 ± -999	0.2532 ± 0.0087	0.5305 ± 0.0119
2459282.5358342	2267.5 ± 10.6	11 ± 15	9.8555	45	0.1412 ± 0.0041	-5.1246 ± 0.145	0.2665 ± 0.0074	0.5166 ± 0.0103
2459539.7731663	2231.6 ± 10.9	48 ± 16	10.0306	44	0.1836 ± 0.0047	-4.5648 ± 0.0608	0.1945 ± 0.007	0.5304 ± 0.0105
2459545.7659941	2043.8 ± 12.8	-15 ± 18	9.5975	36	0.238 ± 0.0062	-6.2329 ± 3.4563	0.2811 ± 0.01	0.5237 ± 0.0123
2459590.7117932	1786 ± 13.9	41 ± 19	9.807	33	0.2119 ± 0.0067	-4.6104 ± 0.1074	0.2212 ± 0.0112	0.5304 ± 0.0152
2459644.7122898	2181.7 ± 14.5	-104 ± 20	9.5813	32	0.2234 ± 0.0066	-4.6445 ± 0.2152	0.3935 ± 0.0129	0.5021 ± 0.0141
2459649.629842	2140.1 ± 10	-118 ± 15	9.8357	49	0.1979 ± 0.0041	-999 ± -999	0.2381 ± 0.0065	0.4922 ± 0.0091
2459652.6796063	2016 ± 12.1	104 ± 17	9.7958	39	0.2288 ± 0.0057	-4.5995 ± 0.0931	0.3102 ± 0.0094	0.5146 ± 0.0116
2459657.727332	1724.3 ± 13	-101 ± 18	10.1905	36	0.1698 ± 0.005	-999 ± -999	0.3019 ± 0.0097	0.5582 ± 0.0127
2459661.6841378	1910.5 ± 16.9	-109 ± 18	10.0861	38	0.24 ± 0.0062	-999 ± -999	0.2641 ± 0.0095	0.538 ± 0.0127
2459662.6697007	1817.8 ± 15.2	83 ± 21	10.0149	30	0.2389 ± 0.0064	-999 ± -999	0.3149 ± 0.0112	0.5291 ± 0.0141
2459685.5096644	2094.7 ± 11.7	-106 ± 17	9.8454	41	0.1575 ± 0.0047	-5.2897 ± 0.36	0.3526 ± 0.0094	0.5028 ± 0.0106
2459687.5617665	2190.1 ± 10.1	-120 ± 15	10.0629	49	0.1979 ± 0.0048	-4.9255 ± 0.1053	0.3099 ± 0.0079	0.4911 ± 0.0098
2459691.5839601	2311.2 ± 14.5	106 ± 20	9.8589	32	0.2592 ± 0.0073	-4.8472 ± 0.2618	0.4324 ± 0.0136	0.4913 ± 0.0144
2459704.623859	2092 ± 15.2	-148 ± 21	9.914	30	0.1667 ± 0.0054	-999 ± -999	0.5008 ± 0.0121	0.5023 ± 0.0128
2460031.6812879	2174.8 ± 11.7	0 ± 17	9.9468	41	0.2287 ± 0.006	-999 ± -999	0.2467 ± 0.009	0.5173 ± 0.0123
2460035.6102046	2142.3 ± 9.8	-60 ± 15	9.8799	50	0.1402 ± 0.0047	-4.7232 ± 0.0919	0.239 ± 0.006	0.5235 ± 0.0088
2460047.6196292	2185.9 ± 11.3	-29 ± 16	9.8589	42	0.1388 ± 0.0075	-6.2879 ± 4.636	0.2799 ± 0.0081	0.5235 ± 0.0109
2460049.6297281	2235.2 ± 11.7	-11 ± 17	9.9268	41	0.1787 ± 0.0048	-4.5127 ± 0.133	0.2593 ± 0.0081	0.5182 ± 0.0105
2460053.5979115	2273 ± 10.3	-28 ± 15	9.8936	47	0.1627 ± 0.0042	-4.6646 ± 0.0912	0.2688 ± 0.0072	0.4967 ± 0.0094
2460064.5861888	2101.8 ± 14	-7 ± 19	10.0588	33	0.215 ± 0.0065	-4.6949 ± 0.1573	0.3868 ± 0.0117	0.5458 ± 0.0134
2460067.4999667	1900.5 ± 12.5	12 ± 18	10.1785	38	0.1855 ± 0.0056	-4.7865 ± 0.1005	0.475 ± 0.0112	0.54 ± 0.0121
2460100.5511551	1911 ± 14.1	-213 ± 18	10.2172	36	0.198 ± 0.0073	-4.0598 ± 0.0348	0.3902 ± 0.0125	0.4311 ± 0.0126
2460404.6178393	1978.3 ± 10.4	-60 ± 15	9.9642	47	0.1620 ± 0.0044	-5.0872 ± 0.2347	0.3396 ± 0.0081	0.5046 ± 0.0100
2460407.5764817	1909 ± 11	68 ± 16	9.8798	44	0.1485 ± 0.0044	-5.1868 ± 0.2541	0.3106 ± 0.0082	0.5284 ± 0.0108
2460411.5489370	1878.9 ± 12.9	90 ± 18	9.9523	36	0.1684 ± 0.0054	-5.0893 ± 0.2633	0.4273 ± 0.0109	0.4882 ± 0.0116
2460433.5833358	2270.6 ± 20.6	-159 ± 28	9.6584	21	0.3803 ± 0.0149	-3.9235 ± 0.0538	2.5052 ± 0.0535	0.5286 ± 0.0315

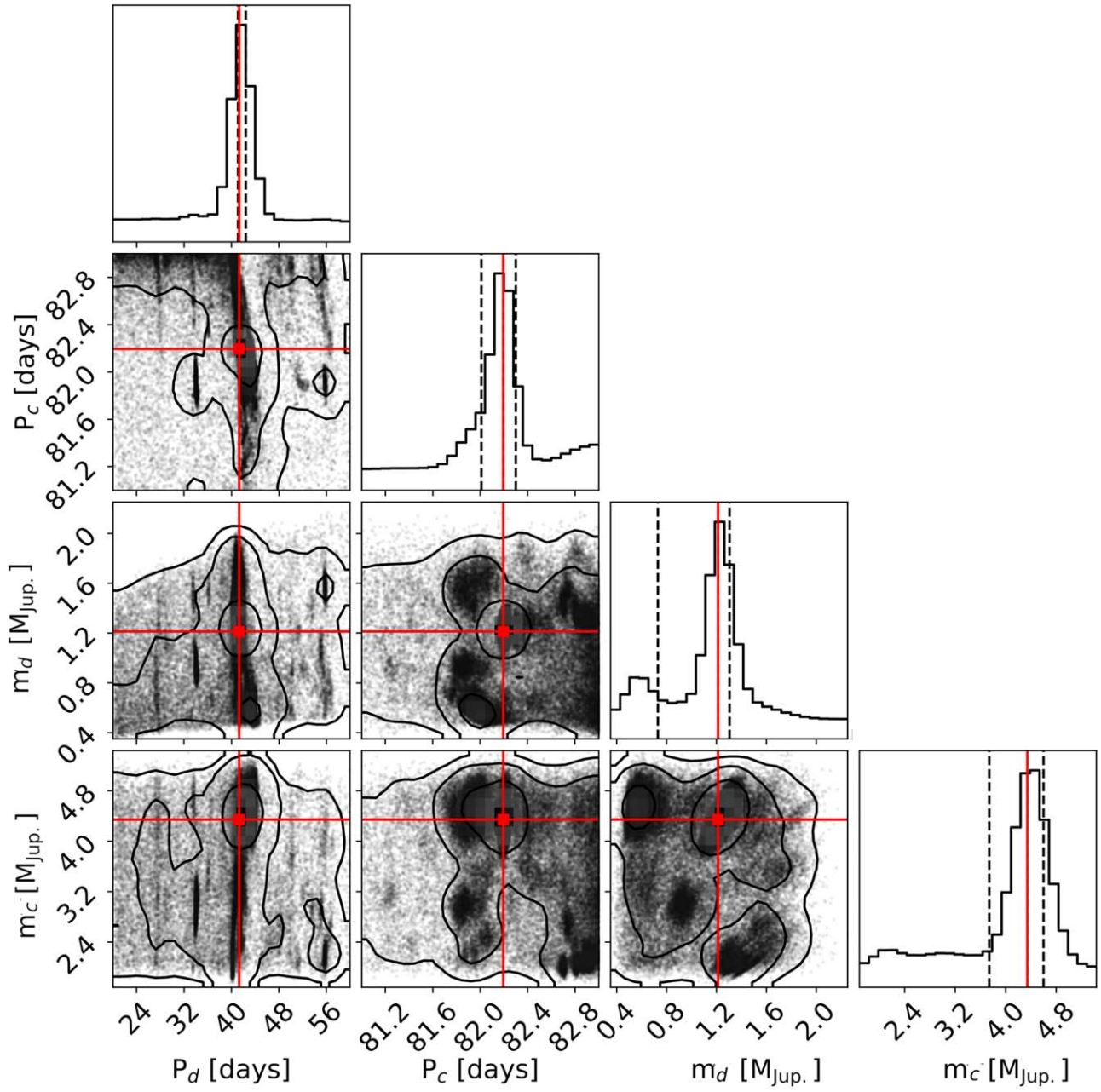


Figure A1. Posterior distribution from a global joint TTV+RV static NS search with very large priors, which aim to map the possible periods for the nontransiting perturber TOI-4504 d. The posterior is multimodal, implying that different period ratios could produce the observed TTVs, but the 41 day period massive planet leads to significantly better fits pointing toward a 2:1 period ratio commensurability with TOI-4504 c.

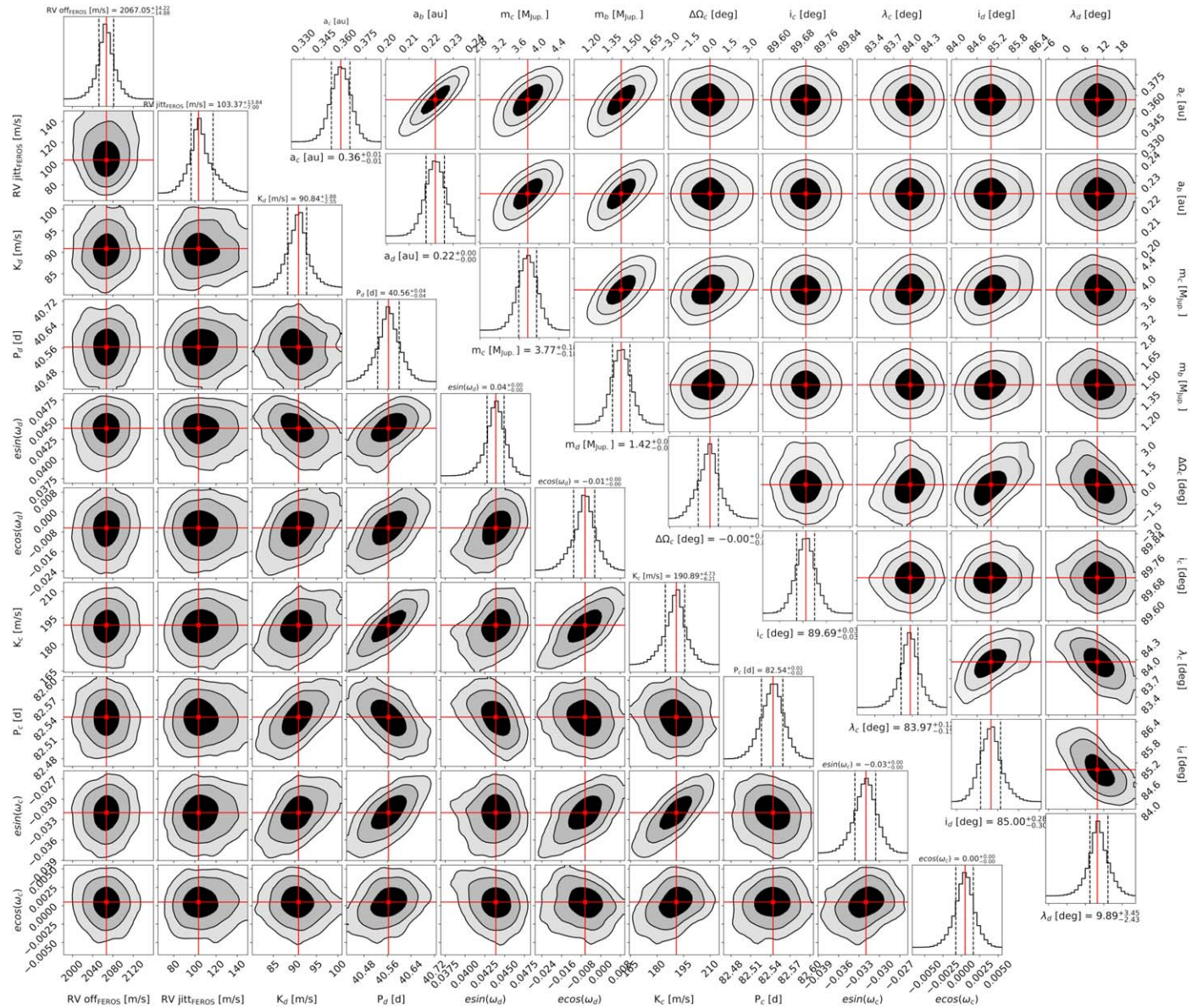


Figure A2. Posterior distribution from a focused joint TTV+RV MCMC sampling, whose results are listed in Table 4. The median values of the fitted and derived posteriors are marked in red. The black contour lines represent the 1σ , 2σ , and 3σ intervals of the distribution.

ORCID iDs

Michaela Vítková <https://orcid.org/0000-0002-2994-2929>
 Rafael Brahm <https://orcid.org/0000-0002-9158-7315>
 Trifon Trifonov <https://orcid.org/0000-0002-0236-775X>
 Petr Kabáth <https://orcid.org/0000-0002-1623-5352>
 Andrés Jordán <https://orcid.org/0000-0002-5389-3944>
 Thomas Henning <https://orcid.org/0000-0002-1493-300X>
 Melissa J. Hobson <https://orcid.org/0000-0002-5945-7975>
 Jan Eberhardt <https://orcid.org/0000-0003-3130-2768>
 Marcelo Tala Pinto <https://orcid.org/0009-0004-8891-4057>
 Felipe I. Rojas <https://orcid.org/0000-0003-3047-6272>
 Nestor Espinoza <https://orcid.org/0000-0001-9513-1449>
 Martin Schlecker <https://orcid.org/0000-0001-8355-2107>
 Maximiliano Moyano <https://orcid.org/0000-0002-7927-9555>
 Susana Eyheramendy <https://orcid.org/0000-0003-4723-9660>
 Carl Ziegler <https://orcid.org/0000-0002-0619-7639>
 Jack J. Lissauer <https://orcid.org/0000-0001-6513-1659>

Andrew Vanderburg <https://orcid.org/0000-0001-7246-5438>
 Karen A. Collins <https://orcid.org/0000-0001-6588-9574>
 Bill Wohler <https://orcid.org/0000-0002-5402-9613>
 David Watanabe <https://orcid.org/0000-0002-3555-8464>
 George R. Ricker <https://orcid.org/0000-0003-2058-6662>
 Roland Vanderspek <https://orcid.org/0000-0001-6763-6562>
 Sara Seager <https://orcid.org/0000-0002-6892-6948>
 Joshua N. Winn <https://orcid.org/0000-0002-4265-047X>
 Jon M. Jenkins <https://orcid.org/0000-0002-4715-9460>
 Marek Skarka <https://orcid.org/0000-0002-7602-0046>

References

- Agol, E., Steffen, J., Sari, R., & Clarkson, W. 2005, *MNRAS*, **359**, 567
 Aller, A., Lillo-Box, J., Jones, D., Miranda, L. F., & Barceló Forteza, S. 2020, *A&A*, **635**, A128
 Baluev, R. V. 2009, *MNRAS*, **393**, 969
 Boisse, I., Moutou, C., Vidal-Madjar, A., et al. 2009, *A&A*, **495**, 959

- Bozhilov, V., Antonova, D., Hobson, M. J., et al. 2023, *ApJL*, **946**, L36
- Brahm, R., Espinoza, N., Jordn, A., et al. 2019, *ApJ*, **158**, 45
- Brahm, R., Jordán, A., & Espinoza, N. 2017a, *PASP*, **129**, 034002
- Brahm, R., Jordán, A., Hartman, J., & Bakos, G. 2017b, *MNRAS*, **467**, 971
- Brasseur, C. E., Phillip, C., Fleming, S. W., Mullally, S. E., & White, R. L., 2019 Astrocut: Tools for Creating Cutouts of TESS Images, Astrophysics Source Code Library, record, ascl:1905.007
- Cabrera, J., Csizmadia, S., Lehmann, H., et al. 2014, *ApJ*, **781**, 18
- Cardelli, J. A., Clayton, G. C., & Mathis, J. S. 1989, *ApJ*, **345**, 245
- Dawson, R. I., Huang, C. X., Brahm, R., et al. 2021, *ApJ*, **161**, 161
- Dawson, R. I., Huang, C. X., Lissauer, J. J., et al. 2019, *ApJ*, **158**, 65
- Deck, K. M., Agol, E., Holman, M. J., & Nesvorný, D. 2014, *ApJ*, **787**, 132
- Dobrovolskis, A. R., & Borucki, W. J. 1996, *BAAS*, **28**, 1112
- Duncan, D. K., Vaughan, A. H., Wilson, O. C., et al. 1991, *ApJS*, **76**, 383
- Espinoza, N., Kossakowski, D., & Brahm, R. 2019, *MNRAS*, **490**, 2262
- Foreman-Mackey, D., Agol, E., Angus, R., & Ambikasaran, S. 2017, *AJ*, **154**, 220
- Foreman-Mackey, D., Hogg, D. W., Lang, D., & Goodman, J. 2013, *PASP*, **125**, 306
- Gaia Collaboration, Prusti, T., de Bruijne, J. H. J., et al. 2016, *A&A*, **595**, A1
- Gaia Collaboration, Vallenari, A., Brown, A. G. A., et al. 2023, *A&A*, **674**, A1
- Gladman, B. 1993, *Icar*, **106**, 247
- Gomes da Silva, J., Santos, N. C., Bonfils, X., et al. 2011, *A&A*, **534**, A30
- Goodman, J., & Weare, J. 2010, *CAMCS*, **5**, 65
- Hobson, M. J., Brahm, R., Jordn, A., et al. 2021, *ApJ*, **161**, 235
- Hobson, M. J., Trifonov, T., Henning, T., et al. 2023, *ApJ*, **166**, 201
- Holczer, T., Mazeh, T., Nachmani, G., et al. 2016, *ApJS*, **225**, 9
- Holmberg, M., & Madhusudhan, N. 2024, *A&A*, **683**, L2
- Huang, C. X., Vanderburg, A., Pál, A., et al. 2020a, *RNAAS*, **4**, 204
- Huang, C. X., Vanderburg, A., Pál, A., et al. 2020b, *RNAAS*, **4**, 206
- Hubbard, W. B., & Marley, M. S. 1989, *Icar*, **78**, 102
- Jenkins, J. M. 2002, *ApJ*, **575**, 493
- Jenkins, J. M., Tenenbaum, P., Seader, S., et al. 2020, Kepler Data Processing Handbook: Transiting Planet Search, Kepler Science Document KSCI-19081-003,
- Jenkins, J. M., Twicken, J. D., McCauliff, S., et al. 2016, *Proc. SPIE*, **9913**, 99133E
- Jones, M. I., Reinarz, Y., Brahm, R., et al. 2024, *A&A*, **683**, A192
- Jordn, A., Brahm, R., Espinoza, N., et al. 2020, *ApJ*, **159**, 145
- Kaufer, A., Stahl, O., Tubbesing, S., et al. 1999, *Msngr*, **95**, 8
- Kempton, E. M. R., Bean, J. L., Louie, D. R., et al. 2018, *PASP*, **130**, 114401
- Kley, W., & Nelson, R. P. 2012, *ARA&A*, **50**, 211
- Korth, J., Chaturvedi, P., Parviainen, H., et al. 2024, *ApJL*, **971**, L28
- Kreidberg, L. 2015, *PASP*, **127**, 1161
- Lee, M., & Peale, S. 2003, *ApJ*, **592**, 1201
- Lee, M. H. 2004, *ApJ*, **611**, 517
- Lee, M. H., & Peale, S. J. 2002, *ApJ*, **567**, 596
- Li, J., Tenenbaum, P., Twicken, J. D., et al. 2019, *PASP*, **131**, 024506
- Lightkurve Collaboration, Cardoso, J. V. d. M., Hedges, C., et al., 2018 Lightkurve: Kepler and TESS time series analysis in Python, Astrophysics Source Code Library, ascl:1812.013
- Madhusudhan, N., Sarkar, S., Constantinou, S., et al. 2023, *ApJL*, **956**, L13
- Millholland, S., Laughlin, G., Teske, J., et al. 2018, *AJ*, **155**, 106
- Miranda-Escudé, J. 2002, *ApJ*, **564**, 1019
- Müller, S., Baron, J., Helled, R., Bouchy, F., & Parc, L. 2024, *A&A*, **686**, A296
- Nelder, J. A., & Mead, R. 1965, *CompJ*, **7**, 308
- Nesvorný, D., Kipping, D., Terrell, D., et al. 2013, *ApJ*, **777**, 3
- Nesvorný, D., Kipping, D. M., Buchhave, L. A., et al. 2012, *Sci*, **336**, 1133
- Noyes, R. W., Hartmann, L. W., Baliunas, S. L., Duncan, D. K., & Vaughan, A. H. 1984, *ApJ*, **279**, 763
- Paegert, M., Stassun, K. G., Collins, K. A., et al. 2022, *yCat*, **4039**, 0
- Panichi, F., Goździewski, K., Migaszewski, C., & Szuszkiewicz, E. 2018, *MNRAS*, **478**, 2480
- Paxton, B., Bildsten, L., Dotter, A., et al. 2011, *ApJS*, **192**, 3
- Paxton, B., Cantiello, M., Arras, P., et al. 2013, *ApJS*, **208**, 4
- Pecaut, M. J., & Mamajek, E. E. 2013, *ApJS*, **208**, 9
- Pepe, F., Cristiani, S., Rebolo, R., et al. 2021, *A&A*, **645**, A96
- Queloz, D., Henry, G. W., Sivan, J. P., et al. 2001, *A&A*, **379**, 279
- Ricker, G. R., Winn, J. N., Vanderspek, R., et al. 2015, *JATIS*, **1**, 014003
- Rivera, E. J., Lissauer, J. J., Butler, R. P., et al. 2005, *ApJ*, **634**, 625
- Schlecker, M., Kossakowski, D., Brahm, R., et al. 2020, *ApJ*, **160**, 275
- Skilling, J. 2004, in AIP Conf. Proc. 735, Bayesian Inference and Maximum Entropy Methods in Science and Engineering, ed. R. Fischer, R. Preuss, & U. V. Toussaint (Melville, NY: AIP), 395
- Smith, J. C., Stumpe, M. C., Van Cleve, J. E., et al. 2012, *PASP*, **124**, 1000
- Speagle, J. S. 2020, *MNRAS*, **493**, 3132
- Stassun, K. G., Oelkers, R. J., Paegert, M., et al. 2019, *AJ*, **158**, 138
- Stumpe, M. C., Smith, J. C., Catanzarite, J. H., et al. 2014, *PASP*, **126**, 100
- Stumpe, M. C., Smith, J. C., Van Cleve, J. E., et al. 2012, *PASP*, **124**, 985
- Tan, X., Payne, M. J., Lee, M. H., et al. 2013, *ApJ*, **777**, 101
- Tayar, J., Claytor, Z. R., Huber, D., & van Saders, J. 2022, *ApJ*, **927**, 31
- Tingley, B., Palle, E., Parviainen, H., et al. 2011, *A&A*, **536**, L9
- Tokovinin, A. 2018, *PASP*, **130**, 035002
- Trifonov, T., 2019 The Exo-Striker: Transit and Radial Velocity Interactive Fitting Tool For Orbital Analysis And N-body Simulations, Astrophysics Source Code Library, Record, ascl:1906.004
- Trifonov, T., Brahm, R., Espinoza, N., et al. 2021, *ApJ*, **162**, 283
- Trifonov, T., Brahm, R., Jordán, A., et al. 2023, *AJ*, **165**, 179
- Twicken, J. D., Catanzarite, J. H., Clarke, B. D., et al. 2018, *PASP*, **130**, 064502
- Wisdom, J., & Holman, M. 1991, *AJ*, **102**, 1528
- Zechmeister, M., & Kürster, M. 2009, *A&A*, **496**, 577
- Ziegler, C., Tokovinin, A., Briceo, C., et al. 2019, *ApJ*, **159**, 19